Conceptual design of the Compact Photon Source for Hall D (Technical Note)

Pavel Degtiarenko,[1] Vitaly Baturin,[2] Hovanes Egiyan,[1,*] Timothy Whitlatch,[1] Moskov Amaryan,[2] Mikhail Bashkanov,[3] Eugene Chudakov,[1] Sean Dobbs,[4] Richard Jones,[5] James Ritman,[6] Justin Stevens,[7] Igor Strakovsky,[8] and Bogdan Wojtsekhowski[1]

[1] *Thomas Jefferson National Accelerator Facility, Newport News, Virginia 23606, USA*

[2] *Old Dominion University, Norfolk, Virginia 23529, USA*

[3] *Department of Physics, University of York, Heslington, York, Y010 5DD, UK*

[4] *Florida State University, Tallahassee, Florida 32306, USA*

[5] *University of Connecticut, Storrs, Connecticut 06269, USA*

[6] *IKP, Forschungszentrum Jülich, D-52428 Jülich GmbH, Germany*

[7] *College of William and Mary, Williamsburg, Virginia 23185, USA*

[8] *The George Washington University, Washington, District of Columbia 20052, USA*

(Dated: July 25, 2023)

This document describes the conceptual design for the high intensity Compact Photon Source (CPS) for Hall D at Jefferson Lab. The Compact Photon Source will serve as both a photon beam source and an electron beam dump located inside the Tagger Hall of Hall D. The photon beam from the CPS will be used to produce a tertiary beam of long lived neutral kaons from a beryllium target located approximately 65 m downstream of the CPS radiator. The presented design is mostly driven by the requirements presented in PAC48 proposal [1] such that it can operate at 5 μA of the 12 GeV electron beam current from CEBAF, producing a photon bremsstrahlung beam in the 10% radiation-length radiator located upstream of the CPS. The design features will allow us to run the experiment at 60 kW of beam power without failures due to thermal effects while meeting the requirements of the radiation control group

of Jefferson Lab.

* Corresponding author; hovanes@jlab.org

CONTENTS

I. INTRODUCTION

The physics program proposed by the KLF collaboration in Hall D relies on the presence of K_L-beam to measure the differential cross sections and self-polarization of strange hyperons on proton and deuteron targets, as well as to study the strange meson spectroscopy in pion-kaon interactions. In order to achieve these goals, a special facility has been proposed to produce a tertiary K_L-beam line at Hall D of the Thomas Jefferson National Accelerator Facility [1]. The flux of this beam will be three orders of magnitude higher than that previously obtained at SLAC.

The K_L-beam with momenta within the range of $0.2 - 10$ GeV is produced in the photoproduction process of neutral kaons from the beryllium target of the Kaon Production Target (KPT) assembly located ~ 24 m upstream of the GlueX detector of Hall D, as described in Ref. [2]. The photon beam is produced in the Compact Photon Source (CPS) located approximately 65 m upstream the KPT. These bremsstrahlung photons of CPS are produced in the thin radiator located just in front of a dipole magnet, similar to Hall C CPS design presented in Ref. [3]. After passing through the thin radiator, the electrons are bent downwards by a dipole magnet and are absorbed in a specially designed copper absorber. The photon beam continues traveling in a straight line through a narrow beam channel towards the Kaon Production Target. The whole setup is surrounded by several layers of various radiation protective materials.

The proposed current for the 12 GeV electron beam is 5 μA, and the radiator thickness required for the expected figure of merit is 10% of a radiation length [1]. With such parameters, the photon beam is expected to carry approximately 5.7 kW of power into the Collimator Cave of Hall D, while CPS will absorb the deflected electron beam with approximately 54.3 kW of power. The KLF experiment is expected to run for 200 PAC days which translates into 4800 PAC hours.

The research and development conducted for Hall C version of the CPS showed that, even at absorbed power on the level of ~ 27 kW, the copper insert may have areas with high temperature. In order to reduce the power deposition density in the Hall D version of CPS where the total beam power is going to be a factor of two larger, we will use a weaker magnetic field and longer distances for electrons to travel in order to reduce the power deposition density in the absorber with respect to the Hall C version. While Hall C CPS

design uses a magnet with non-uniform magnetic field with a maximum field of $B \sim 3.2$ T [3], Hall D version will use a simpler dipole magnet with a field of approximately $B \sim 0.67$ T which produces shallower angle of impact and smaller power deposition densities at the absorber. Hall D model also uses lead shielding instead of tungsten which increases both the longitudinal and the transverse size of CPS compared to the Hall C version, but it significantly reduces the cost. Although having a large device is usually not desirable, the larger size allows us to separate the magnet and the absorber from each other, which should significantly simplify the design of both components as well as of the whole device.

Studies that we performed allowed us to create a conceptual design that we strongly believe will work for the KLF experiment. Subsequent detailed mechanical design and optimization process will provide more details on the parameters of the CPS and a better cost estimate for it. In particular, in the next stages of the process we will need to optimize quantities like the temperature of the absorber, the related mechanical stresses, and the radiation dose rates versus the cost of the CPS.

II. MAIN COMPONENTS OF HALL D CPS

We used the conceptual design of Hall C CPS [3] as the starting point for our own development. At the core of Hall C CPS, which is about 2.1 m long and approximately 1.8 m $\times$ 1.8 m wide in the cross section, is a magnet with 60 cm-long coils that can provide up to three-Tesla non-uniform magnetic field. Electron beam of Hall C going through a narrow horizontal channel is deflected downwards by the magnetic field, and it eventually reaches and interacts with the walls of the beam channel, creating an electromagnetic shower at a location referred in this document as the hot spot. As a result, most of the electron beam energy is deposited in the copper absorber, all within the length of the bending magnet. The magnet assembly with the absorber are inside multiple shielding layers made of tungsten, lead, and borated polyethylene. Although this design has obvious advantage of being compact to allow for an installation in relatively narrow spaces, there is a number of disadvantages associated with it. Hall C CPS magnet has a complex design with chamfered poles made of expensive high-permeability material, and the poles and the coils of the magnet are in relative proximity to the interaction area of the beam and the absorber, which would limit the lifetime of the coils unless special care is taken when selecting the

insulation material of the coils. In addition, the small size of the interaction region in the copper core results in temperatures above 500°C which potentially can produce stresses and deformation in the absorber. And finally, in order to make the overall dimensions of the Hall C CPS small, a large amount of tungsten is used for radiation shielding in the areas around the absorber, which significantly increases the price of the device. We build upon the experience gained by the Hall C CPS core group to design a different version of compact photon source that would be optimal for the KLF experiment and well-suited for Hall D Tagger Hall.

The model presented in this note is the result of pursuing several approaches to the conceptual CPS design, starting with the one presented in the original KLF proposal, then investigating and trying to apply the novel approaches based on the well-developed CPS concept for the experiments at Hall C of Jefferson Lab and modifying it for the KLF. Studying previous approaches and further developing them for KLF proved to be very useful in the end to develop a balanced and suitable solution. The limitations to the overall dimensions of the CPS for the KLF facility are less strict, so the new solution does not need bulk tungsten shielding, and only needs it in few critical small volumes. Significant efforts were dedicated by the KLF collaboration to pursue this direction of development, extending the longitudinal dimension of the CPS, but keeping a sweeping magnet close to the locations of the significant beam power deposition. Using one narrow beam opening both as the photon exit channel and the beam dump may result in significant radiation streaming down the line, both in the form of photons and charged particles (electrons and positrons in dynamic equilibrium with the photons). The solution proposed in this document and illustrated in Figs. 1 and 2 increases the aperture for the photon beam, removes the need for a second electrical magnet at the downstream end of the CPS, and places the first bending magnet at a safer distance upstream of the main beam absorber. The magnet coils are less exposed to the prompt radiation, to the level at which the magnet may become if not serviceable, but replaceable in principle. This is achieved by shortening the length at which the main electron beam is absorbed, resulting in slightly higher maximum temperatures inside the copper absorber.

The Compact Photon Source for Hall D will be located in the Tagger Hall, as shown on Fig. 1. The Tagger Hall currently houses GlueX radiators, the tagger dipole magnet, tagging hodoscope detector [4], and various beam line equipment. The beam dump area

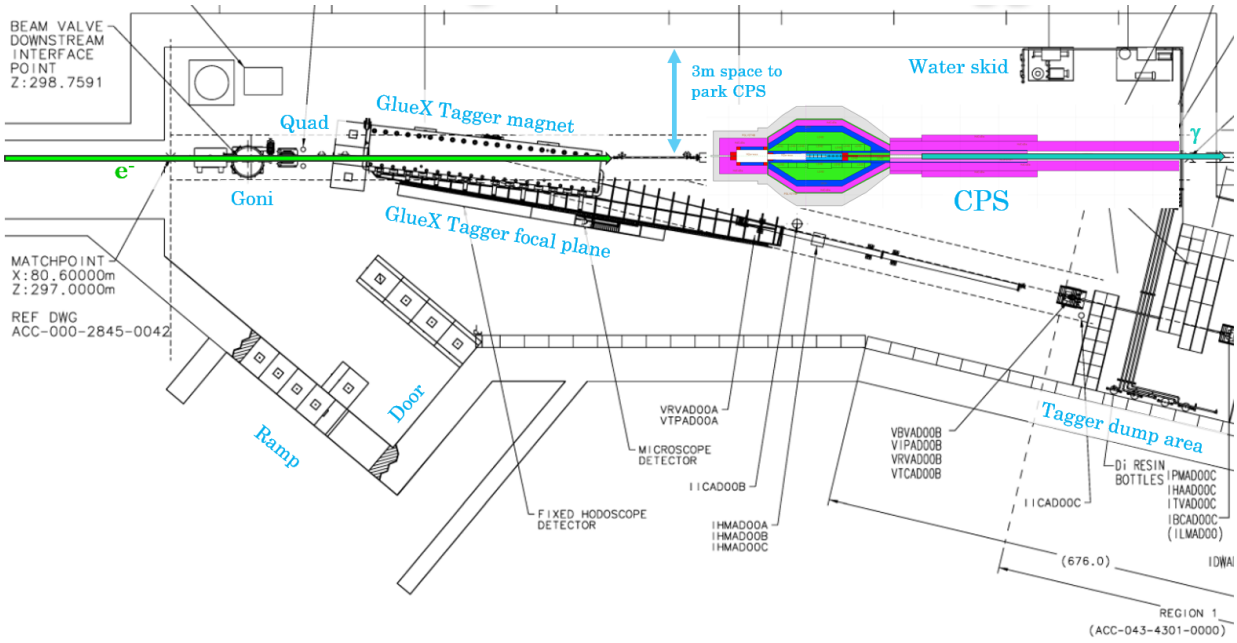

FIG. 1. Engineering drawing of the Tagger Hall with a superimposed FLUKA model of CPS. The tagger magnet and the tagger dump will not be used during KLF experiment.

shown in the right-bottom corner of Fig. 1 that has been used with the nominal tagged photon beam configuration for GlueX will not be used during the KLF experiment. The CPS will be installed downstream of the tagger magnet and the existing permanent magnet will be moved further downstream closer to the east wall of the Tagger Hall. During KLF experiment the GlueX radiators will be removed and the tagger magnet will be degaussed and de-energized so that the electron beam travels downstream in a straight path reaching CPS which will serve as the new photon beam source and as the new electron beam dump.

In this note, we present the conceptual design of Hall D CPS, and we show that such a design satisfies the requirements of the radiation safety of Jefferson Lab. The FLUKA model of the CPS in Figure 2 shows the horizontal view of the midplane vertical slice of the CPS for an observer located at the beam-right side. Similar to Hall C, the Hall D version of compact photon source will use a magnet followed by a long copper absorber that acts as an electron beam dump. The role of the electrical dipole magnet, which is located immediately after the radiator, is to bend the primary electron beam as well as the electrons that produced the photons out of the photon beamline into the specially designed copper absorber where the electron beam will be terminated and all its remaining energy will be dumped. The existing permanent magnet is attached at the downstream end of the CPS to clean the remaining

charged particles produced in the electromagnetic showers, and to provide magnetic field in case of the power supply failure of the first magnet. The magnets, the radiator, and the absorber are enclosed in multiple layers of radiation shielding to keep the radiation levels within the limits defined by the radiation control group of Jefferson Lab. The CPS will be movable in the horizontal direction so that we can restore the photon beamline aperture by moving the whole assembly to the north of the beamline once the KLF data taking is complete. More studies will need to be performed to optimize the geometry of this device, the amount of the shielding, the costs, and the required cooling, after which the engineering design will commence.

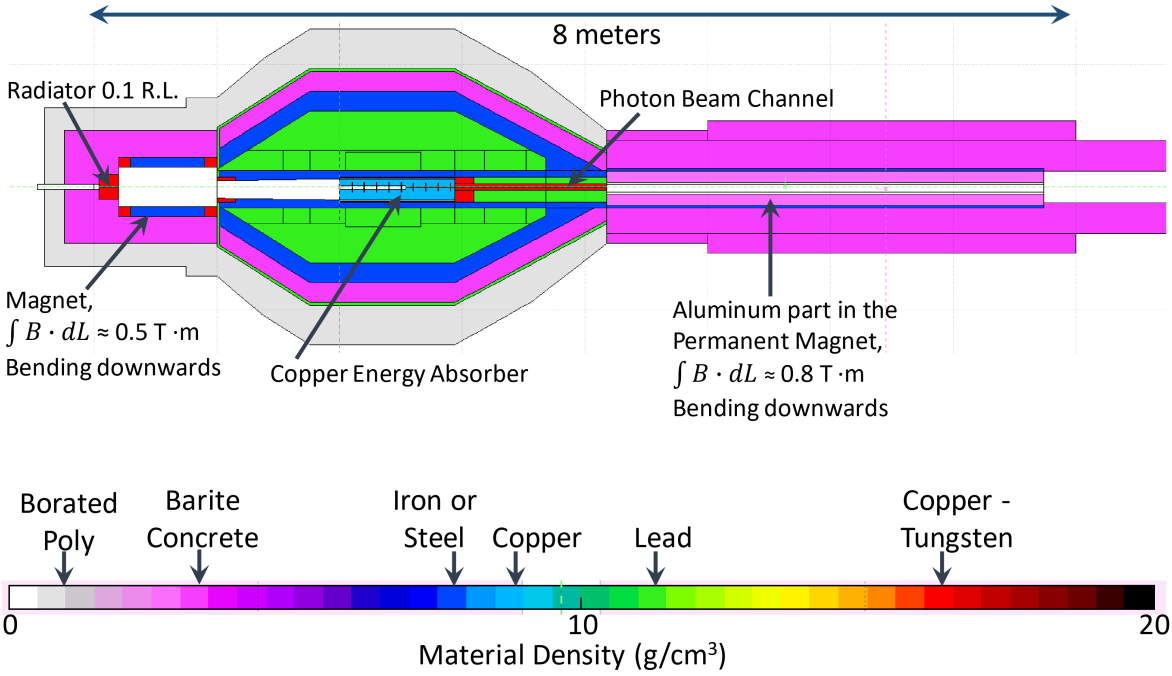

FIG. 2. Rendering of the CPS model for KLF by FLUKA. The color of the regions represents the density of the material.

A. Radiator for photon production

KLF experiment requires a radiator with a thickness of 10% of a radiation length to produce a sufficient photon flux to create $\sim 10^4$ kaon per second rate at the location of the cryogenic target [1] inside the GlueX detector. The simplest option for the radiator is to use a 1.4 mm thick copper plate or foil due to the low magnetic permeability and the

high thermal conductivity of copper. As the beamline vacuum will end just upstream of the copper radiator, we will have a very small additional amount of photon bremsstrahlung from the thin vacuum window typically amounting to approximately 0.1% of a radiation length.

In order to facilitate the beam tuning procedure for KLF, it would be highly desirable to have a remotely removable radiator. This should not excessively complicate the mechanical design because the CPS beam channel does not need to be held under vacuum. We plan to have a retractable radiator system that will have a blank position, a thin radiator on the order of 10^{-3} of a radiation length copper, and the production radiator of 10% of a radiation length.

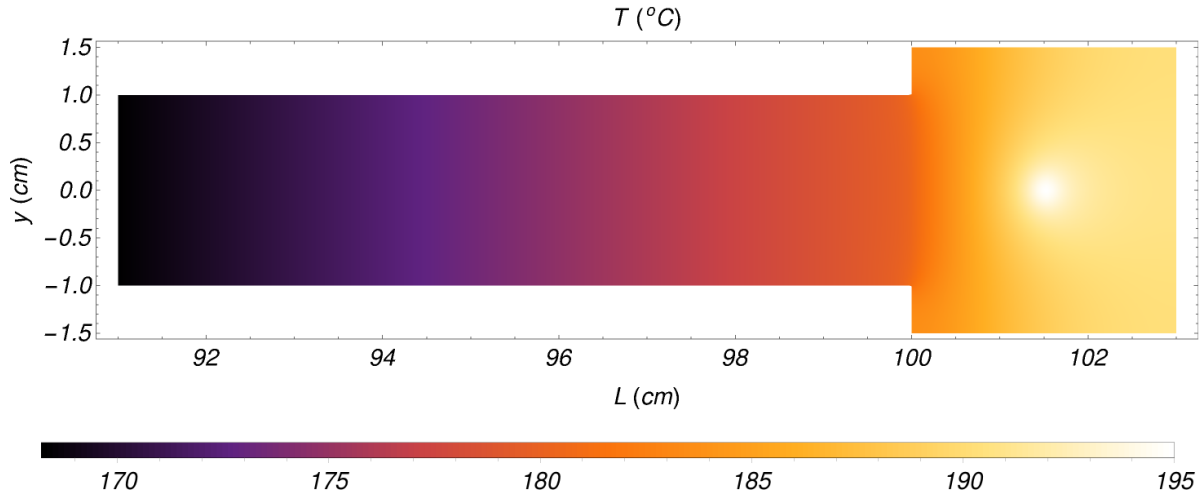

FIG. 3. Radiator temperature in the plane transverse to the beam direction in a model where there is no heat losses via convection or radiation. The horizontal axis is the distance from the cooling point. The color indicates the temperature in °C. The assumed length for the radiator holder stick is one meter. See text for details.

Power deposition in the photon radiator is expected to be on the order of 10 W only, based on our FLUKA simulations. In order to assess potential problems related to thermal effects in the radiator, we estimated the temperature distribution using a simple model for the radiator and the holder. For these calculations, we assumed that the radiator is a square plate with sides of 3 cm in length attached to a one-meter long copper stick with the cross section of 2 cm $\times$ 1 cm. We also assumed that the 10 W of power is distributed according to a Gaussian distribution with a radial width of $\sigma = 1$ mm in the transverse plane, and a uniform distribution in the direction of the beam. Without any thermal contact to an external body, the only cooling mechanisms would be convection and radiation, and the

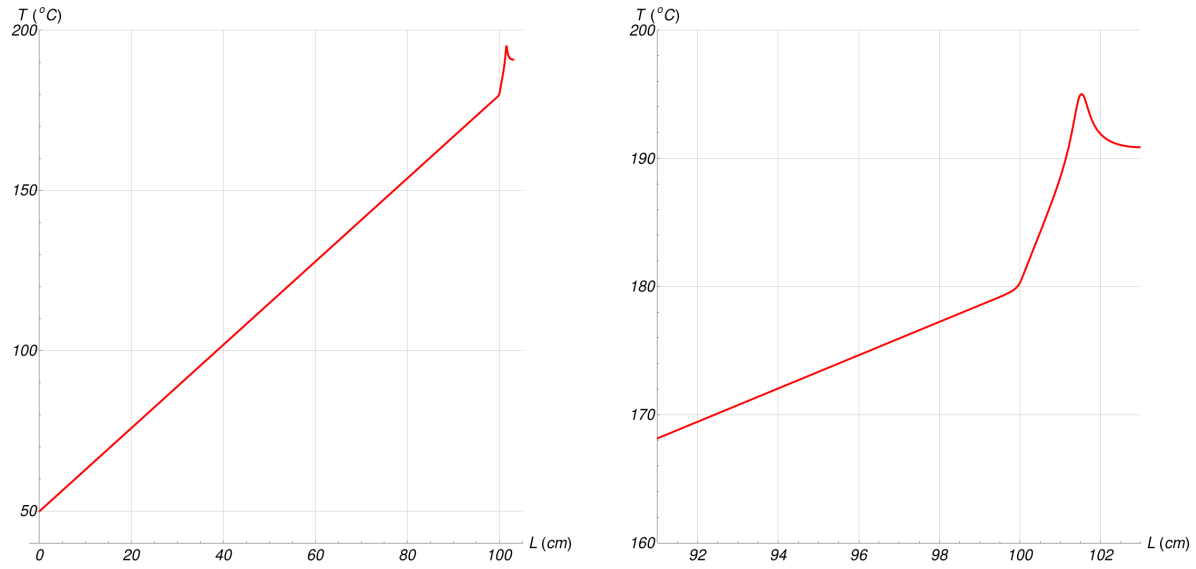

FIG. 4. Radiator temperature at the center of the radiator holder versus the length from the cooling point. The assumed length for the radiator holder stick is one meter. See text for details.

radiator temperature could potentially increase up to 400°C. Since we will have a remotely-controllable radiator ladder, there will be heat flow from the radiator through the arm of the motion system. Figure 3 and Figure 4 show the temperature distributions in such a simplified radiator assembly model where the only heat dissipation is through heat conduction through the holder, which is assumed to be kept at a fixed temperature of 50°C at the other end. The horizontal axis in both Figures 3 and 4 is the distance from the cold end of the stick. One can see that the temperature difference across the face of the radiator itself will be small, on the level of 20°C, and most of the temperature drop will arise from the way the radiator plates are supported. For the assumed copper stick, the temperature at the beam spot will be approximately 200°C. The temperature difference at both ends of the radiator holder arm linearly depends on its transverse cross section. Therefore, making the holder twice thicker will reduce the radiator temperature with respect to the cold end of the stick by almost a factor of two. Note, that at these temperatures the radiator will also dissipate power of approximately 2 Watts via heat radiation and convection through the nitrogen or air in the electron beam channel, therefore the temperature at the center of the radiator will be even lower.

The actual radiator holder will be attached to an actuator that will allow us to remotely control which radiator is in the electron beam. The mechanical design of the holding stick will need to be sufficiently stiff and will need to have sufficient thermal conductivity to

prevent the radiator assembly from deforming. Although our current rough estimate of 200°C is significantly lower than the melting temperature of the copper, it would be more desirable to keep it as cool as reasonably possible. We will optimize the radiator assembly during the engineering design stage when all the parameters of the radiator assembly will be determined with a much better accuracy.

B. Magnets

For Hall D CPS, we can use a relatively weak horizontal magnetic field created by a relatively short coil packages located at the upstream end of the beam channel. The magnetic field will deflect the beam electrons by a few milliradians with respect to its original direction along the z-axis so that they hit the bottom of the beam channel in the middle of a long copper absorber.

It is quite obvious that the larger the interaction area of the beam with the absorber is, the lower the power deposition density will be. The size of the beam spot in the absorber depends on the multiple factors, such as the bending magnetic field, distance from the magnet, the vertical size of the beam opening of the absorber. For a very short magnet and small magnetic field integral $\int B\ dl$, the longitudinal spread of the beam spot on the absorber is defined by the vertical beam size and by the location of the spot along the beam axis. The location of the center of the hot spot linearly depends on the channel size and it also can be controlled by adjusting the magnetic field. One can make the location of the hot spot closer to the radiator by increasing the magnetic field integral $\int B\ dl$, which would decrease the longitudinal size of the hot spot.

To illustrate this, one can imagine a parallel electron beam going through a thin radiator followed by a magnet, followed by a very long rectangular beam opening, as illustrated in schematics in Fig. 5. Using the formula for the deflection angle of electrons in a magnetic field, we can write:

$$\delta\phi = 0.3\ \frac{\int B\ dl}{P}\ , \tag{1}$$

where $\delta\phi$ is the deflection angle of the beam in radians, $\int Bdl$ is the field integral in units of $\mathrm{T}\cdot\mathrm{m}$, and P is the electron momentum in units of GeV/c . Then from the geometry, we

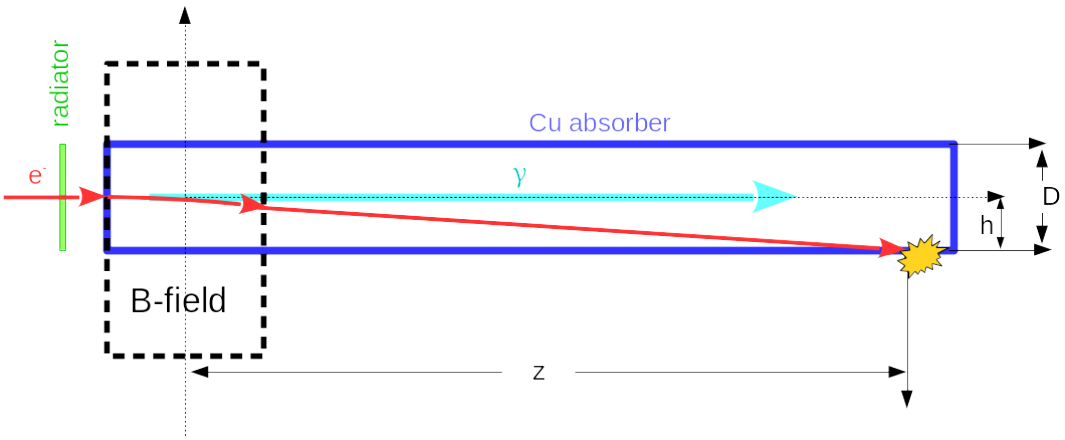

FIG. 5. Schematics illustrating the basic concept for creation of the bremsstrahlung beam with a radiator and deflecting the electron beam downward using a weak dipole magnet. The distances are not to scale.

get the following expression for the z-position and the size in σ_z of the beam spot on the absorber:

$$z = \frac{L_M}{2} + \frac{1}{0.3}\,\frac{P}{\int B\,dl}\,(h - \Delta h_s)\,, \tag{2}$$

and

$$\sigma_z = \frac{1}{0.3}\,\frac{P}{\int B dl}\,\sigma_h\,, \tag{3}$$

where z is the location of the beam spot on the absorber with respect to the center of the magnet in meters, L_M is the length of the magnetic field area, σ_z is longitudinal size of the hot spot, h is the vertical distance from the beam center to the bottom of the beam channel, and σ_h represents the size of the original electron beam in the vertical direction, as illustrated Figure 5. In Eq. (2), Δh_s is the amount in vertical position change of the electron at the exit of the magnet, and for a dipole field one could use an approximation $\Delta h_s \sim 0.15\,\frac{L_M^2 B}{P}$ measured in meters . Also, in Eq. (3), we assumed that the path integral $\int Bdl$ is constant for all electrons in the beam, which is the case for a uniform constant magnetic field. In addition to the intrinsic electron beam size, the dispersion of the beam, the angular spread of the electrons due to the finite beam emittance, and the multiple scattering in the radiator will further increase the size of the hot spot in the absorber. The energy losses in the radiator will also create a tail of deposited power upstream of the main hot-spot.

Using Eq. (3), one can see that the longitudinal size of the hot spot size can be increased by reducing the magnetic field. For that reason the magnetic field used in Hall D design is significantly weaker than what Hall C version will use, which allows us to mitigate the issues of the larger power deposition densities in the copper absorber. Also, one can estimate that if we use a magnetic field with $\int B\ dl \approx 0.4\ \mathrm{T}\cdot\mathrm{m}$, and a vertical electron beam size is $\sigma_h \approx 1$ mm, then the longitudinal hot spot size on the absorber will be $\sigma_z \approx 10$ cm. That is, approximately 95% of the energy for the electrons that did not produce photons is expected be deposited in a 40 cm long section of the absorber. Equations (2) and (3) also show that if one changes the beam channel's vertical size and adjusts the magnetic field to keep the location of the hot spot center constant, one could also change the vertical size of the electron beam by the same relative amount to keep the maximum power deposition density in the absorber approximately the same.

Although the absorber shape that we propose in this note is more complex than discussed above, the argument that the power density deposition in the areas of the absorber with a uniform channel along the beam direction can be reduced by lowering the magnetic field, still holds. As it is shown in the following sections of this note, we performed careful studies using FLUKA [5] simulations and ANSYS [6] calculations to verify that we indeed can spread the absorbed power of the electron beam into a large enough volume of the absorber such that the resulting temperature in the CPS core does not exceed 300° C.

The magnetic field provided by the CPS magnet needs to be in the horizontal direction and perpendicular to the beam direction such that the trajectories of the beam electrons bend downwards as they travel through the magnet. Although it is not critical for the magnetic field to be uniform, using a dipole field simplifies the design of the magnets as well as of the whole device. Geometrical constraints on the CPS magnet are such that a sufficient horizontal space is available in-between the poles for the beam to pass through without interacting with the poles and without creating excessive radiation dose for the coils. Also, it is desirable to have the outer dimensions of the magnet yoke as small as possible because the magnet is expected to be surrounded by shielding layers that add to the weight and to the cost of the device. Currently we are considering dipole magnets that can fit within a square of 50×50 cm^2 in the transverse direction and have a gap size of at least 1 cm. We used OPERA [7] to design a prototype of a dipole magnet satisfying these criteria. Figure 6 shows the overall features of a simple dipole magnet with physical

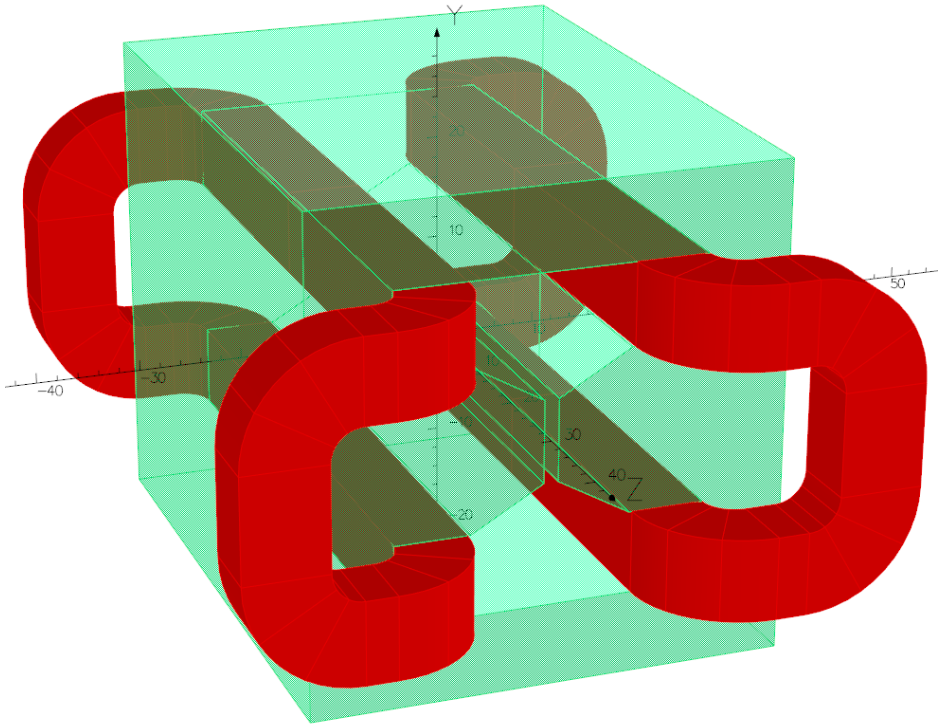

FIG. 6. OPERA rendering of a dipole magnet with a 1.4 cm gap and 60 cm long bedstead coils. The red color shows the location of the magnet coils. The translucent green color represents the iron yoke and the poles of the magnet.

lengths of 80 cm, that has transverse size of the yoke is 46 cm $\times$ 48 cm in the horizontal and vertical directions, respectively, and a 1.4 cm gap size between the poles. The total length of the bedstead coil package along the z-axis is 80 cm to provide a uniform field area of approximately 60 cm in the straight region of the coils. The bedstead configuration of the coils was chosen to keep the coils away from the beamline even at the coil return location to minimize the radiation exposure.

The horizontal component of the magnetic field B_x calculated using OPERA software package [7] versus y and z coordinates with respect to the center of the magnet is shown on the left panel of Fig. 7. The right panel shows the dependence of B_x on the z-coordinate along the $(x = 0, y = 0)$ central line. One can see that the field is very uniform in z between $z = -30$ cm and $z = +30$ cm and has small tails beyond these points. We used the field map produced by this simple model for the FLUKA simulations described in Section III.

Figure 8 shows the absolute value of the magnetic field in the transverse plane in the center of the magnet with $z = 0$ calculated using OPERA [7] software package. The areas of the 8 cm thick yoke and the chamfered poles can be clearly identified. The largest magnetic

field is at the corners of the poles and it is below 1 Tesla in magnitude, which is well below of iron saturation point.

From this exercise one can conclude that we can get near 0.67 T magnetic field with a current density of $\sim$ 67 A/cm^2 flowing through the copper coils of cross section area of 54 cm^2 using a magnet of these dimensions. Assuming forty turns for the coils, this would amount to 93.8 A current from the power supply to the coils. The exact current in the coils would have to be determined based on the electron beam energy and will depend on the final shape of the copper absorber and its location.

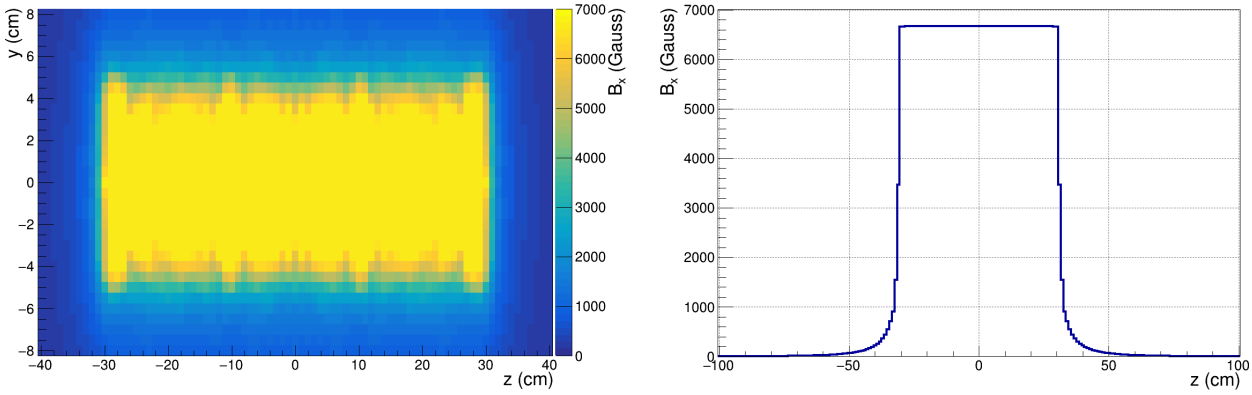

FIG. 7. Horizontal component of the magnetic field calculated using OPERA simulation program for the model shown in Fig. 6 . Left panel shows the horizontal component B_x of the magnetic field versus y- and z-coordinates at $x = 0$ vertical plane. The right panel shows B_x versus z-coordinate along the $(x = 0, y = 0)$ central line.

One of the important considerations for the CPS magnet is the radiation hardness of the magnets coils. The radiation is caused by the secondary particles emitted from the photon radiator as well as from the showers produced in the copper absorber downstream. Such radiation may damage the coil insulation of the magnet coils, and, therefore, needed to be studied. The current CPS design assumes that the downstream edge of the magnet is one meter upstream of the upstream edge of the copper absorber where the electron beam first starts interacting with it. Our simulations performed using FLUKA software package [5] show that the accumulated radiation dose near the coils is expected to be on the level of $\sim 3 \times 10^4$ Gy, which should be safe for the full duration of the experiment, as argued in Section V D. As a result of our studies, we came to conclusion that such a magnet can be readily designed by the Physics Division's magnet group or by a private company as the requirements for it are not very restrictive.

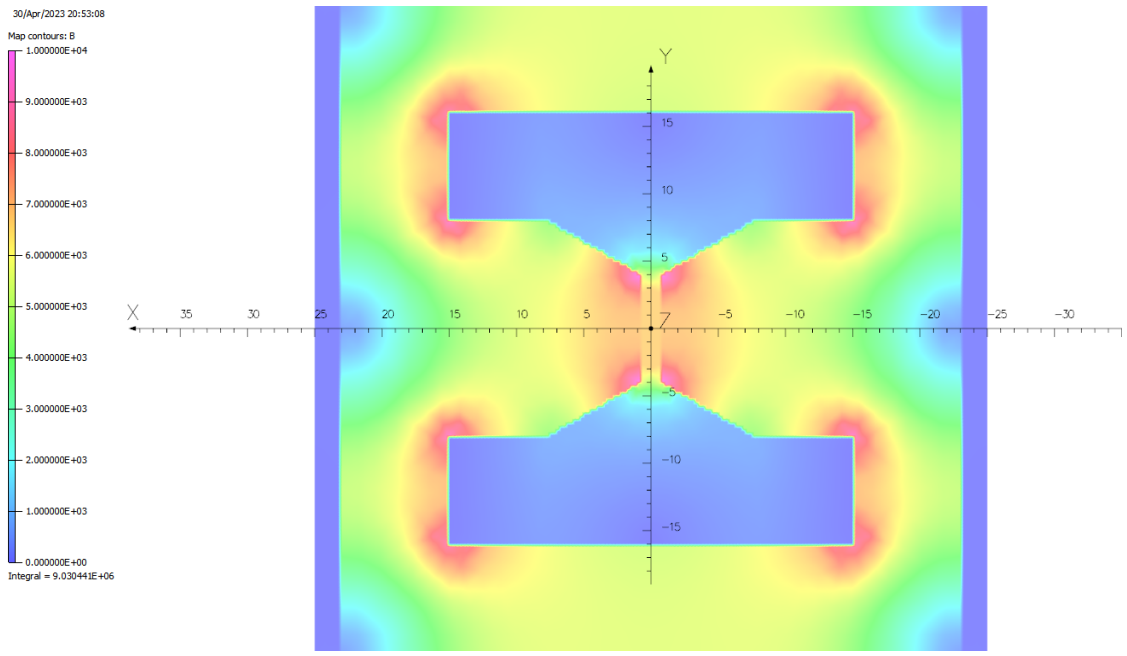

FIG. 8. Magnitude of the magnetic field in the transverse plane $z = 0$ at the center of the magnet shown in Fig 6, calculated using OPERA simulation program.

In addition to the new magnet located before the copper absorber, we will also utilize the permanent magnet currently used in Hall D for GlueX photon beam. This is a Vertical Bend Dipole magnet, referred to as a PDV magnet, and it is made at FNAL [8]. It is 140 inches long and it has bending power of 0.822 $\mathrm{T} \cdot \mathrm{m}$. The only current purpose for this magnet is to bend electron beam downward if the tagger magnet is suddenly turned off to prevent the electrons from getting into the main Hall. During KLF experiment this magnet will be moved further downstream to create space for CPS, and it will be used to clean the photon beam from charged particles as well as to bend the electron beam downward in case the upstream electrical magnet trips.

C. Absorber

One of the key components of CPS is its copper core designed to absorb most of the shower energy produced by the electron beam and to disperse it over a large volume from which the heat will be removed using a water cooling system. We chose copper as the preferred material because of its high thermal conductivity, relatively high melting point, low magnetic permeability, and its low cost. Based on our FLUKA simulations described

in the following sections, approximately 53.5 kW of power is expected to be deposited in the absorber area. Therefore, one could expect high temperatures in some areas of the absorber if the heat is not removed from there. In order to keep the temperature of the the absorber well below the melting point of copper and to avoid large thermal stresses and deformation, chilled water will circulate through the channels inside or on the outer surface of the absorber, and it will be handled by the same closed-loop water handling system used for the tagger dump as it has been certified for 5 μA beam current at 12 GeV. The number and the locations of the cooling channels will be determined during the engineering design.

The absorber in the proposed model is a 94 cm long rectangular copper block with height and width of 20 cm that has a beam channel of varying cross section going through it. Figure 9 shows a three-dimensional model of the absorber where one can see the the beam channel and the 5 mm wide vertical slits positioned at 10 cm distance from each other along the beam direction to minimize the thermal deformations and thermal stresses during beam operations . Figure 9 also shows the potential locations of four cooling tubes with radii of $r = 1.2$ cm located diagonally 9.9 cm from the central axis and running parallel to the beamline. Alternatively, the absorber can be cooled using water running through copper tubings brazed on the whole outside surface of the absorber, or by using eight cooling pipes inside the absorber. Potentially, such an absorber can be manufactured from two separate pieces split in the center by a vertical plane. The exact cooling configuration, the size, the number, and the locations of the slits, as well as the method for the manufacturing and machining of such an absorber will be determined during the engineering design stage. In order to have a good estimate of the impact of the heat from the electron beam deposited in the absorber, we used ANSYS [6] and Wolfram Mathematica [9] programs using power deposition distributions from FLUKA simulations as an input. The details of the simulations of the heat deposition and the temperature calculations in the absorber are presented in Section III and Section IV, respectively.

The beam channel in the copper core starts with a relatively large entrance cavity that follows a large drift section of the CPS in front of the absorber filled with air or nitrogen, where not much power deposition is expected. The top part of this cavity looks like a cylinder with a radius of 1 cm, while the bottom part looks like a wedge with slightly rounded bottom. The shape of this part of the channel is chosen such that the bottom of the channel acts like a wedge that narrows as the electrons travel downwards, such that the power deposition is

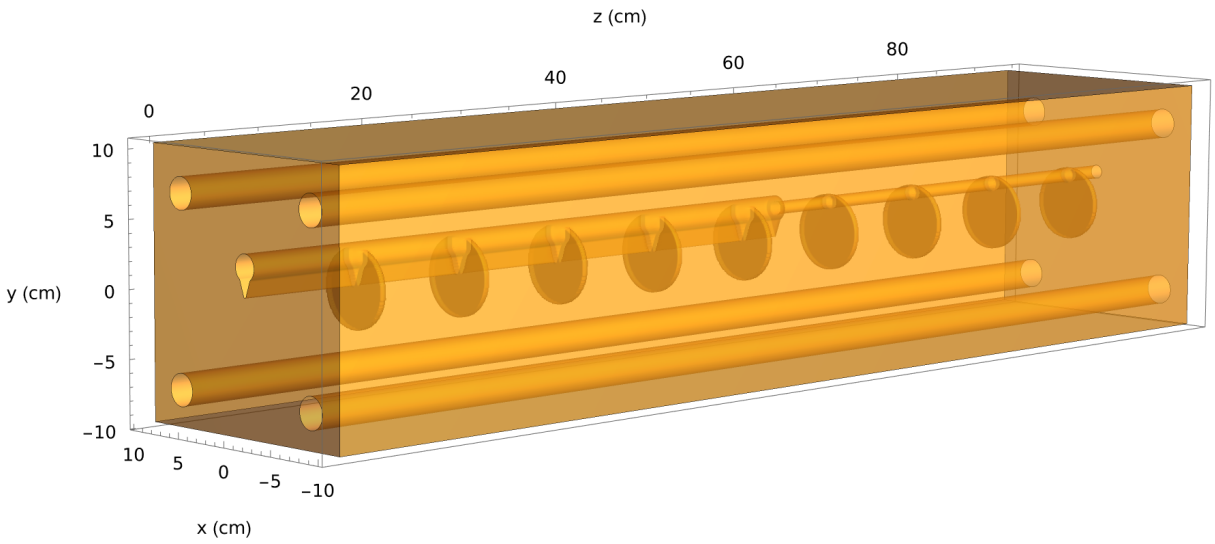

FIG. 9. Rendering of the copper absorber of CPS as implemented in Wolfram Mathematica [9] model.

spread in all directions along the walls of the wedge. After the wedge-shaped cavity, there is a narrower conical photon beam channel with a circular cross section centered around the line that the primary electron beam would have followed without the bending magnet. The conical photon channel starts at $z = 54$ cm and continues to the downstream end of the absorber. The diameter of this part of the beam channel is 1 cm at the very beginning, and it increases slightly along the beam axis to minimize the secondary particle production off of the walls of the channel. The remnants of the electromagnetic showers produced by the interactions of the electron beam with the absorber walls in the previous wider cavity are expected to be blocked from traveling down the photon channel by the vertical wall at the lower part of the downstream end of the beam entrance cavity, thus trapping most of the secondary particles inside the absorber.

D. Shielding

As mentioned previously, the CPS will not only act as the photon beam source but also as the electron beam dump located inside the Tagger Hall. Therefore, it is important to ensure that the prompt radiation levels in the Tagger Hall are low enough not to damage the equipment present in the hall during the experiment, not to interrupt the experiment due single event upsets in the electronics, and to avoid detectable radiation above the Tagger

Hall berm. It is also important to have low activation levels around CPS so that we can access the Tagger Hall to service the equipment during the experiment without long delays. The criteria that we use for designing the shielding for CPS is such that the prompt radiation in the Tagger Hall during KLF experiment is similar to what is currently expected to have for GlueX beamline configuration using 20 μm diamond radiator with 5 μA electron beam current [1]. We also require that the Tagger Hall is available for servicing equipment within one hour of turning the beam off during the experiment, although some areas in the immediate vicinity of the CPS may not be accessed for a prolonged period of time.

Most of the beam energy is deposited near the center of the copper insert inside the CPS producing a shower that propagates outwards further into the CPS. In order to contain the radiation within the CPS we propose using multiple layers of shielding. The resulting radiation environment is described in Section V.

III. FLUKA SIMULATIONS

FLUKA simulation package [5] is the natural choice for modeling and optimizing the design of the CPS. It offers good accuracy describing bulk electromagnetic (E-M) processes in multi-GeV energy range (better than 5-10%), reasonable description of hadron production processes in high energy particle interactions, including photo- and electroproduction (about 20-30%), and also reasonable description and handling of the material activation at high energies (30-50%). The general layout of the CPS FLUKA model is shown in Fig. 2 and the model placement in the Hall D complex is illustrated in Fig. 10.

The main parts of the proposed CPS conceptual solution as shown in Fig. 2 are the entrance collimator with 10 mm diameter opening for the beam and the 0.1 R.L. copper radiator placed inside, then the beam deflecting $\sim$ 0.5 Tesla $\cdot$ meter magnet with 1.4 cm magnet field gap to avoid beam scattering inside the magnet, then 1 meter long beam entry channel, also formed in the shape of a 1.4 cm slit expanding vertically to allow electrons which lost their energy to the photon production in the radiator to stream down and interact with the absorber. Then there is the copper absorber featuring the entrance cavity to spread the main electron beam and let it be absorbed such that the surface electromagnetic cascading was not directly visible in the photon beam channel which is circular with the diameter of 10 mm in the beginning, and slightly tapered out to let the scattered photons go down along

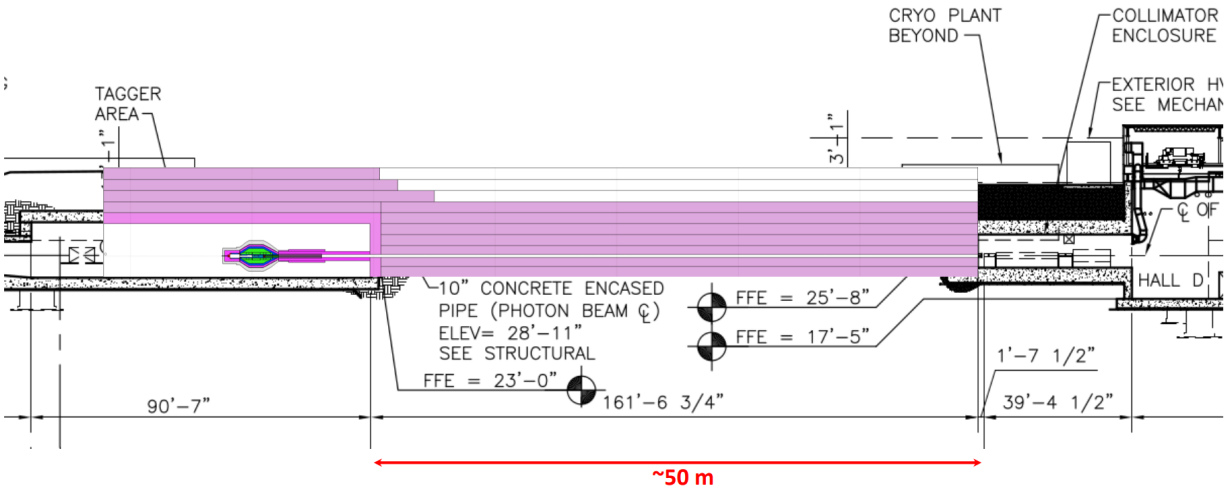

FIG. 10. CPS FLUKA simulation model placement in the Hall D Tagger building, including the model of the photon beam line leading to the Collimator Cave enclosure. The outer surfaces of the shielding layers in the model are cylindrical, but the vertical cut image of the model was cropped in the bottom to allow the visibility and alignment of the model to the Tagger enclosure's floor.

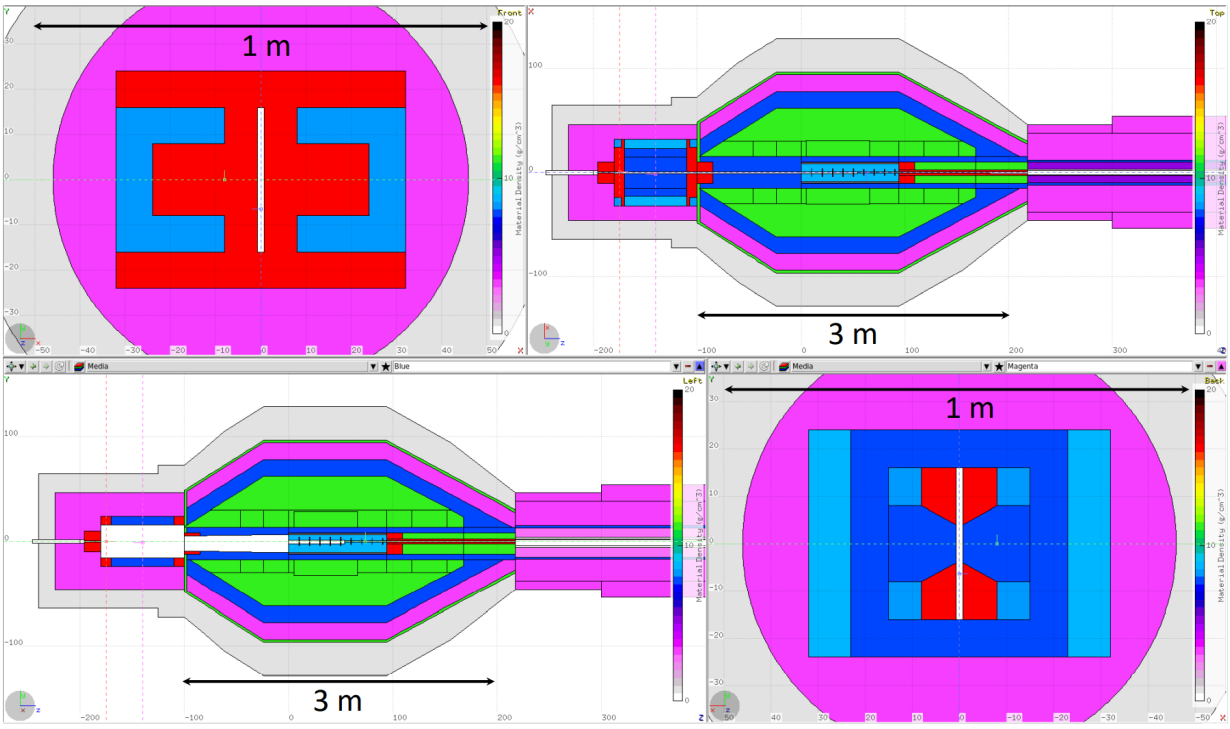

FIG. 11. FLUKA simulation model details of the powered magnet at the CPS entrance. Color map represents density of the materials in the same way as in Fig. 2. See text for details.

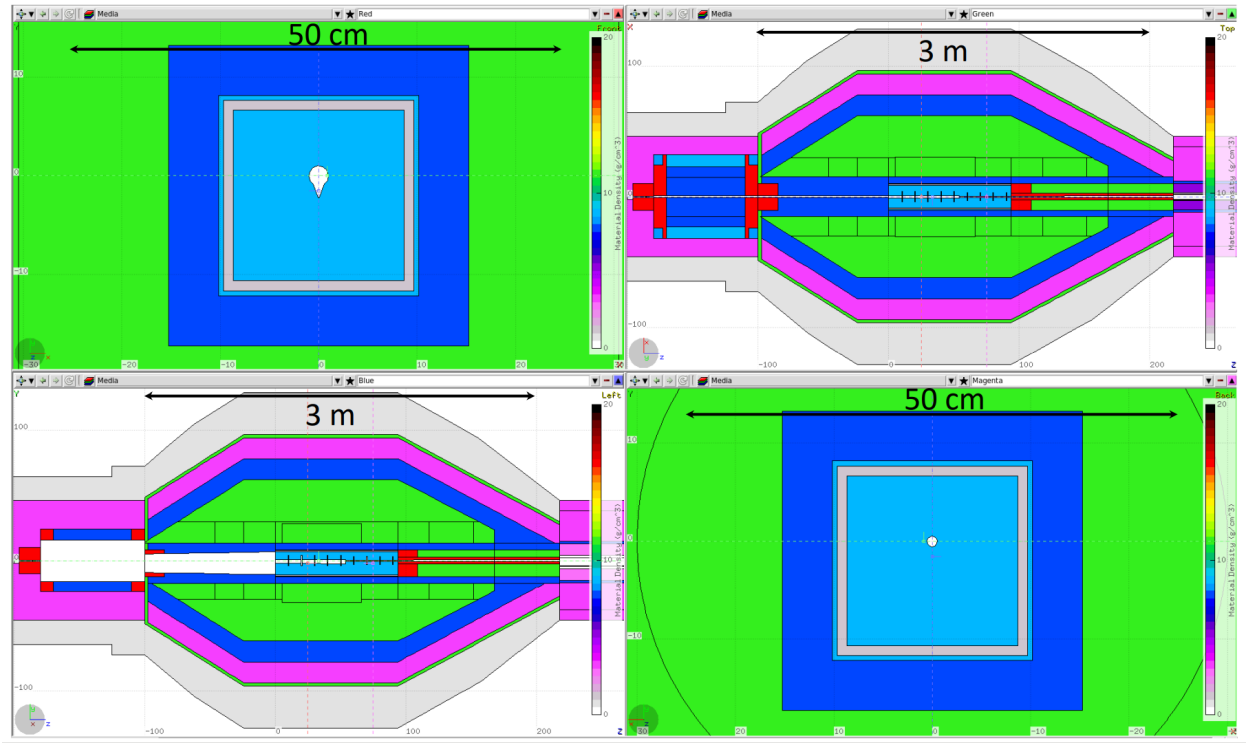

FIG. 12. FLUKA simulation model details of the main CPS body. Color map represents density of the materials in the same way as in Fig. 2 (see text for details).

their path to the Collimator Cave with minimal scattering and cascading. The channel goes through the main absorber, and then continues inside a long block of heavy tungsten-copper material, removing bulk of the electromagnetic cascading in the channel. The last part of the CPS complex in the Tagger Hall is the permanent magnet that is currently present in the beam line and used as the protection against inadvertent full beam delivery into Hall D. In the present configuration, it still serves the same purpose, but also removes the charged particles generated in the electromagnetic cascades in the exit line. All the elements need to be shielded to limit the prompt dose rates in the Tagger Hall enclosure, as well as the levels of radiation coming from the activated materials, to allow safe access to the Tagger Hall enclosure during beam interruptions. The weights of different materials used in the proposed model are given in Table I. The total weight of the CPS in this model, without the magnet, is approximately 75 metric tons.

Figure 11 shows details of the CPS geometry near the entrance to CPS. Top left panel shows the front view of the vertical cut in the beginning of the magnet, showing the copper coils extending outwards in this plane, and heavy tungsten-copper material filling up the

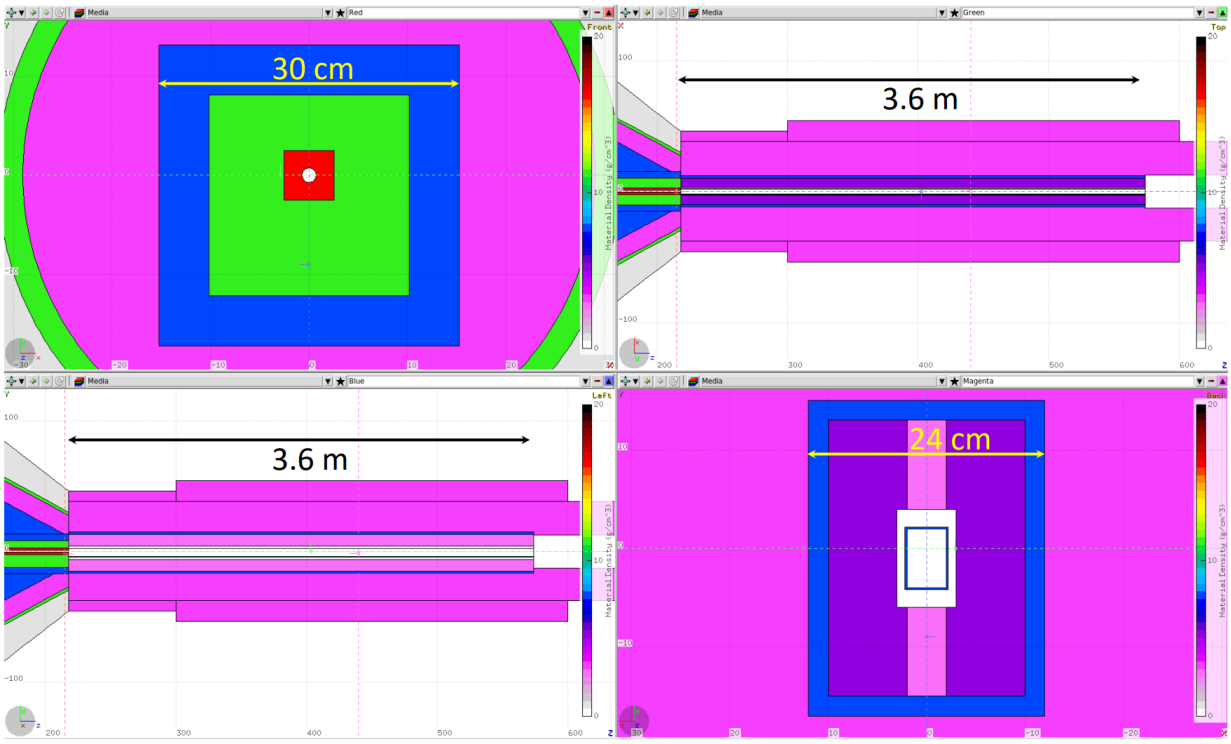

FIG. 13. FLUKA simulation model details of the permanent magnet at the CPS exit. Color map represents density of the materials in the same way as in Fig. 2. See text for details.

Material \ CPS Region	Entry (ton)	Core (ton)	Body (ton)	Exit line (ton)	Total (ton)
Cu20/W80	1.34	0.23	0	0	1.57
Lead	0	0.48	25.73	0	26.21
Copper	0.52	0.35	0	0	0.87
Iron & steel	0.91	1.53	12.51	0	14.95
Barite concrete	1.93	0	7.23	15.87	25.03
Borated polyethylene	1.05	0	5.45	0	6.5
All materials	5.75	2.59	50.92	15.87	75.13

TABLE I. Table of the material weights in metric tons used in the CPS FLUKA simulation model.

space between the coils to protect them from the products of the beam scattering in the collimator and radiator upstream. Top right panel of Fig. 11 shows the horizontal cut of the CPS assembly, bottom left panel shows vertical cut plane of the assembly, including the magnet, and bottom right panel shows the vertical cross section of the magnet, with the iron magnet yoke surrounded by copper fill layers on its left and right, copper coils in the

inner corners, and tungsten-copper inserts protecting the coils, and equipped with the slit for the main and scattered electron beam to pass through.

Figure 12 illustrates the details of the main CPS body, including the copper absorber, photon exit line and other core elements inside the base steel support enclosure, surrounded by the shielding layers of lead, iron, high density barite concrete, lead skin layer, and the outer layer made of borated polyethylene. Color map represents density of the materials in the same way as in Fig. 2. Top left panel shows the vertical cut of the absorber in the middle of the beam entry cavity, designed to accept the full power electron beam along its bottom edge, which provides the surface to spread and absorb the beam along its left, bottom, and right surfaces, diminishing the power density deposited in the material. Bottom right panel shows the vertical cross section of the absorber in the middle of its second part, illustrating the circular opening for the photon beam produced by the CPS.

Figure 13 shows details of the FLUKA model of the CPS in the downstream region of the permanent magnet. Color map represents density of the materials in the same way as in Fig. 2. Top left panel shows the vertical cross section of the assembly just before the end of the main CPS body, showing the photon channel in the copper-tungsten beam exit block, surrounded by the lead shielding in the steel base box, in turn surrounded by the barite concrete layer, the lead skin layer, and the borated poly layer. Top right and top left panels show the horizontal and the vertical cross sections of the permanent magnet at the exit of the CPS, and the bottom-right panel shows the vertical cross-section of the permanent magnet in its middle.

IV. POWER DEPOSITION IN THE ABSORBER

The copper absorber is one of the most critical parts for the CPS design. The shape and the dimensions of the absorber define the temperature distribution in the CPS and the maximum temperature at the hot post. At 12 GeV beam energy and 5 μA beam current, the copper core of CPS may receive as much as 60 kW of power. During nominal running we use a 10 % copper radiator which will reduce the total power received by CPS to 54.3 kW due to the energy carried away by the photon beam. We design Hall D CPS for the nominal running conditions keeping in mind that in the unlikely scenario of removing the radiator while keeping the beam current at 5 μA, the temperature difference between the hottest

spot of the copper core and the surface of cooling tubes will increase by about 10%.

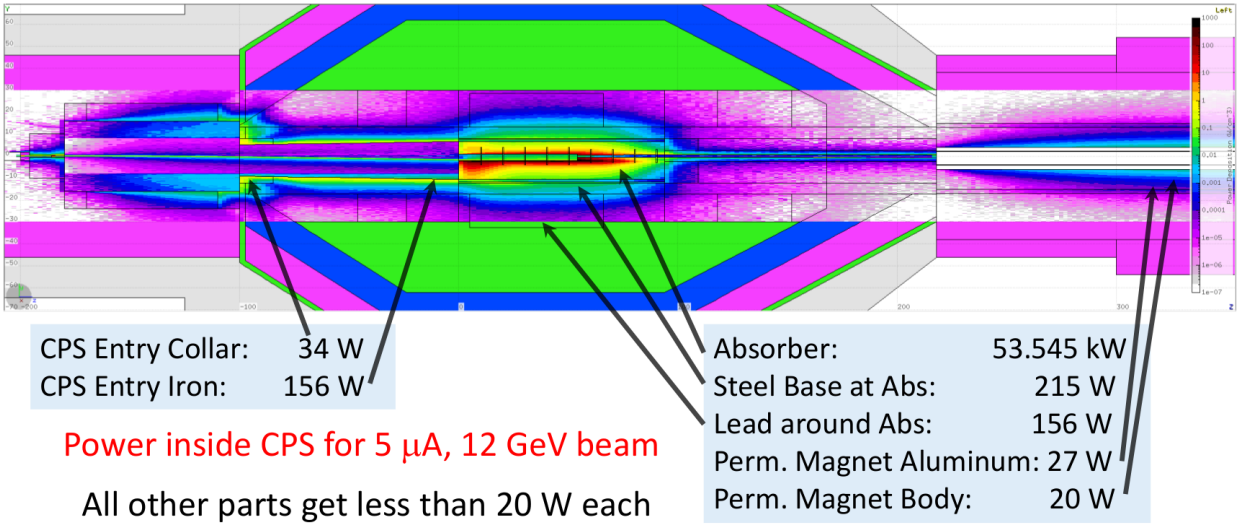

FIG. 14. Power distribution calculated using the FLUKA CPS model under nominal running conditions with 12 GeV, 5 μA electron beam with a Gaussian transverse spread at FWHM = 2.5 mm. The color map superimposed on the CPS geometry in the central core area shows the power density in logarithmic scale ranging from very small levels and up to the values of several kW/cm^3 shown by color red and darker colors. The parts of the CPS model receiving more than 20 W power are listed in the plot.

A. Power Deposition Density

As discussed in Section II B and is illustrated in Fig. 14, almost all of the beam power is expected to be deposited in the absorber. We performed FLUKA simulations to evaluate the power deposition distribution in the absorber in detail using very fine grid in order to understand the effects the absorbed heat will have on it. The resulting power deposition density versus z and y hall coordinates in the vertical midplane is shown in Fig. 15. There is very little power deposited in the area $y > -2.2$ cm and $z < 54$ cm which is the region of the cavity filled with nitrogen or air. Most of the power is deposited in the the range 20 cm $< z <$ 50 cm where the maximum of the temperature distribution is located. Also note that there is a tail in the $z < 10$ cm region which is due to the electrons that lose relatively large amount of energy in the radiator and hit the front end of the absorber at $z = 0$. The vertical gaps in Fig. 15 indicate the locations of the vertical 5 mm slits where very small amount of power is deposited in the gas. The power deposition density distribution

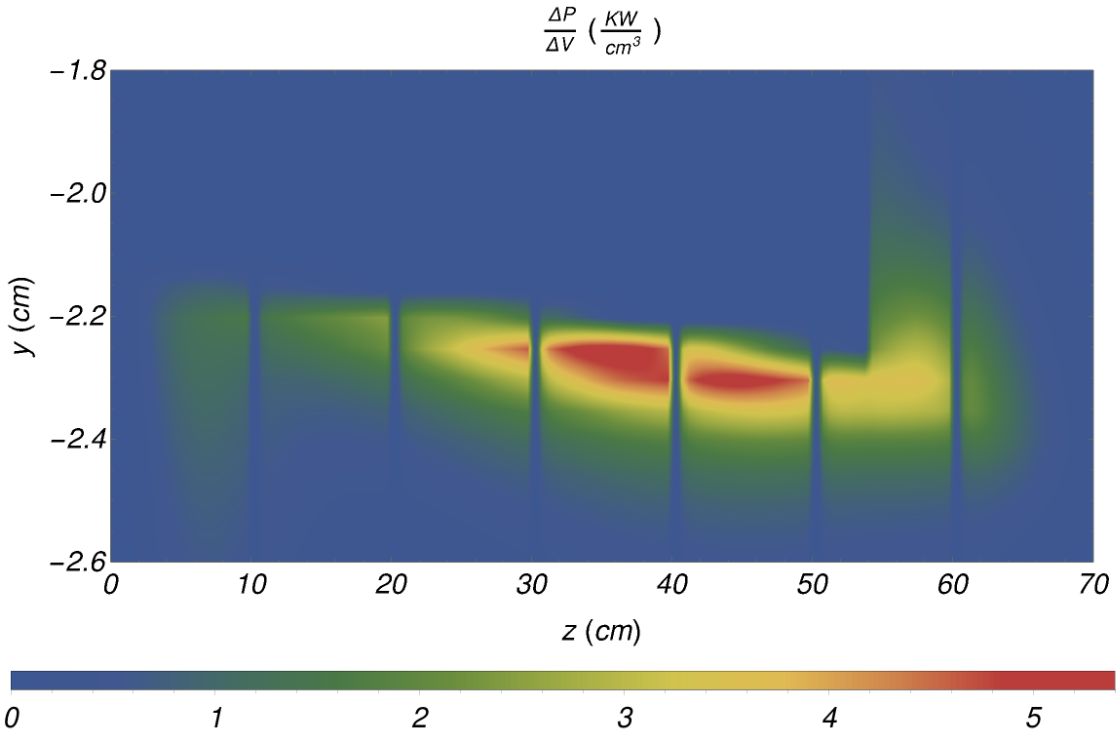

FIG. 15. Power deposition density in the copper core for nominal electron beam configuration versus z- and y-coordinates in the $x = 0$ vertical plane zoomed in near the hot spot area.

versus z along the $x = 0$ and $y = -2.25$ cm is shown on the left panel of Fig. 16. The maximum local power deposition density is at around $z = 37$ cm on that line, and its value is about 5.5 kW cm^{-3}. The right panel of Fig. 16 shows the linear power deposition density versus the z-coordinate, where the transverse coordinates are integrated over. Thus, the largest power is deposited in a narrow disk at $z = 60$ cm with the linear power deposition density of ~ 1.2 kW cm^{-1}.

Figure 17 shows the power absorption distribution in the transverse planes at the hot spot (left) and at the position $z = 55$ cm (right). Note, that the center of the photon beam is along the $(x, y) = (0, 0)$ on these plots. The plot on the left panel is at the z-position of the hottest point of the absorber, and one can clearly see the outlines if the cross section of the relatively large beam cavity for trapping the secondary particles. The most of the power is absorbed at the bottom of the wedge somewhere within the entry part of the beam channel at the nominal beam conditions. The plot on the right panel shows the power deposition density around the circular photon beam channel at $z = 55$ cm. Most of the power at this z-position is still deposited about 2 cm below the center of the photon beam as it is created

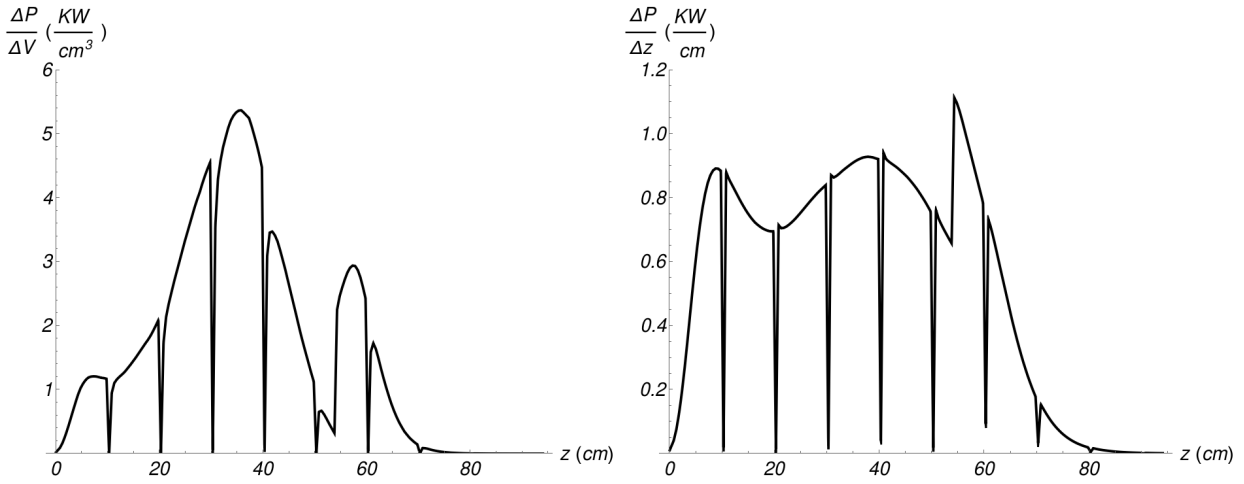

FIG. 16. Power deposition profile in the absorber along the beam direction. The left panel shows the local power deposition density $\frac{\Delta P}{\Delta x \Delta y \Delta z}$ versus z along $(x, y) = (0\text{ cm}, -2.25\text{ cm})$. The right panel shows the linear power deposition density $\frac{\Delta P}{\Delta z}$, where the power density is integrated over the transverse coordinates x and y at each z-position of the whole absorber.

by the electrons at the periphery of the primary electron beam envelope and by the particles from the electromagnetic shower upstream.

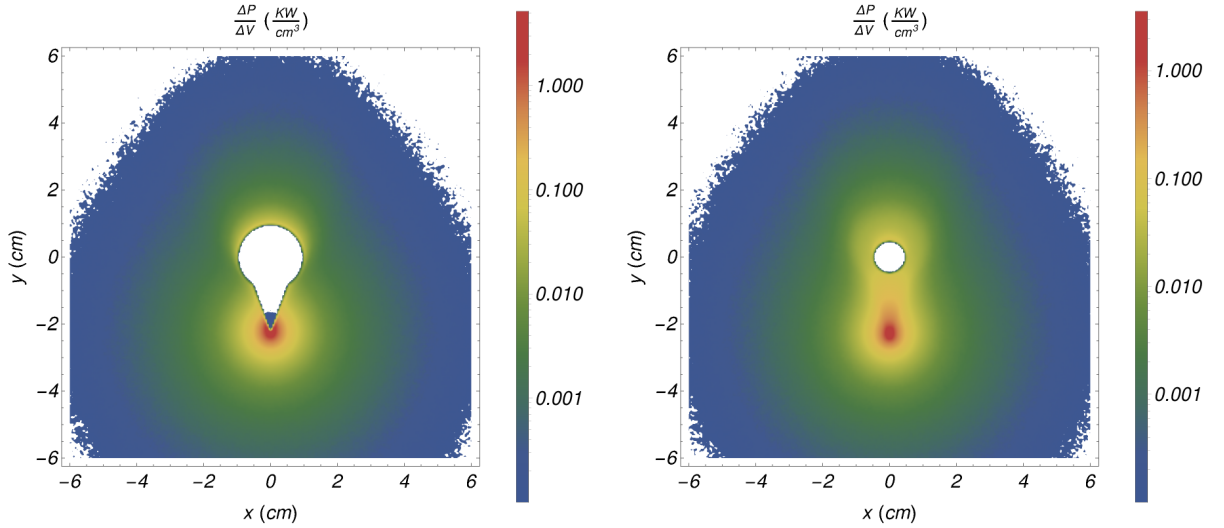

FIG. 17. Power deposition density versus x- and y-coordinates. Left panel shows power deposition density in the wider cavity area at the hot spot $z = 37$ cm plane, while the right panel shows the power deposition density in the photon beam channel at position $z = 55$ cm.

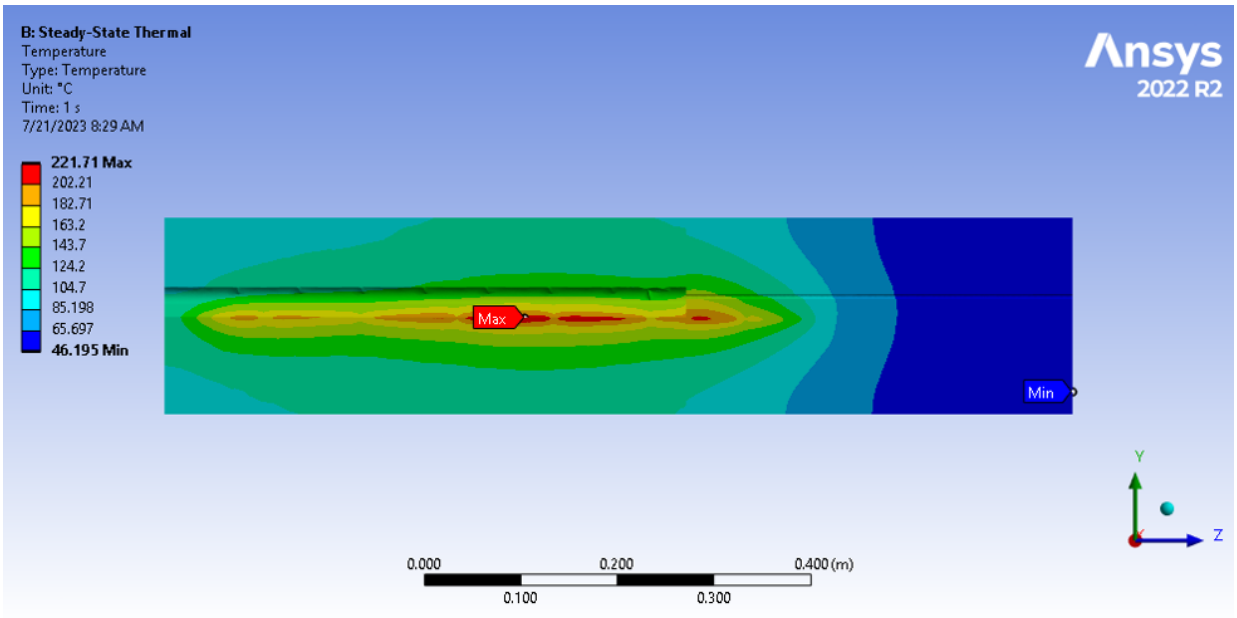

FIG. 18. Temperature distribution inside of the CPS absorber for the nominal electron beam conditions estimated with steady-state thermal analysis using ANSYS [6] software. The temperature at the hottest spot is expected to be around $T_{max} \approx 222°$C.

B. Temperature in the Absorber

Using power absorption distribution maps from FLUKA simulations we evaluated the temperature distribution in the absorber by applying Finite Element Methods (FEM) in the ANSYS [6] and Wolfram Mathematica [9] software packages available at Jefferson Lab. In these calculations we assumed that the only heat flow to and from the absorber is via the surfaces of the cooling pipes and that there is no heat flow through the external surfaces of the absorber. Such an approximation results in a conservative estimate of the temperatures in the copper core as no heat will flow from the other parts of the CPS into the absorber. Figure 18 shows the snapshot from the ANSYS [6] program with the temperature distribution for the nominal beam configuration. These results are in a good agreement with the temperature distributions obtained by solving the heat equation using Wolfram Mathematica [9] shown in Fig. 19. We also estimated absorber temperature distributions not only for the nominal beam condition but also for various beam conditions, see Table II, that would be possible based on the electron beam specification for KLF described in Section VI A. We looked at eleven different beam conditions to understand the dependence of the temperature distribution in the absorber on the primary beam conditions. The conclusion is that the

absorber temperature will not exceed 300 °C if the beam conditions are kept under control. In order to perform such extensive studies, we used Wolfram Mathematica [9] software packages to solve the Poisson equation at the thermal equilibrium with appropriate boundary conditions:

$$-\kappa \, \nabla^2 T(\vec{r}) = q(\vec{r}) \, , \tag{4}$$

where κ is the thermal conductivity of the medium and is assumed constant, $q(\vec{r})$ is the power deposition density distribution, and $T(\vec{r})$ is the temperature distribution in the absorber. The imposed boundary condition were such that the absorber could be considered as an insulated body, and the only heat exchange happened at the location of the water cooling tubes. Therefore, the boundary condition at all surfaces except the cooling pipes are:

$$\vec{\boldsymbol{\nabla}} T \cdot \vec{n} = 0 \, , \tag{5}$$

and the boundary conditions on the surface of the cooling pipes are:

$$\kappa \, \vec{\boldsymbol{\nabla}} T \cdot \vec{n} = -h \, (T - T_W) \, , \tag{6}$$

where h is the heat transfer coefficient between the cooling water and the absorber, and T_W is the cooling water temperature. The power source term in the right-hand-side of Eq. (4) is the power deposition map $q(\vec{r})$ obtained from our FLUKA simulations with fine meshes binned in both cylindrical and rectangular coordinates.

For the temperature calculations in the the copper absorber we assumed thermal conductivity of copper $\kappa = 385 \ \mathrm{W{\cdot}m^{-1}{\cdot}K^{-1}}$ and the heat transfer coefficient $h = 5,000 \ \mathrm{W{\cdot}m^{-2}{\cdot}K^{-1}}$ for the heat exchange across the surface of the cooling pipes. We also assumed an average water temperature of $T_W = 40$ °C ignoring the effects of the water warming up as it flows through the pipes. We estimate that if one provides 30 gallon per minute volumetric coolant flow, then the water temperature will change by less than 10 °C while passing through a single length of the copper absorber. Note, that these assumptions for different parameters depend on the capacity of the chilled water handling system, the type of the copper material, and other choices, and the final implementation of the cooling system in the engineering

Beam configuration	z-location of the hot spot	T_{max}
Nominal beam, no halo	37 cm	230 °C
Narrow beam with $\sigma = 0.33$ mm	43 cm	290 °C
Wide beam with $\sigma = 1.5$ mm	8.5 cm	205 °C
97% magnetic field	56.5 cm	245 °C
103% magnetic field	33 cm	240 °C
Beam shifted by $\Delta x_b = +1$ mm	8 cm	260 °C
Beam shifted by $\Delta y_b = -1$ mm	8.2 cm	220 °C
Beam shifted by $\Delta y_b = +1$ mm	57 cm	265 °C
Beam angled by $\Delta_x \theta_b = +0.5$ mrad	8 cm	260 °C
Beam angled by $\Delta_y \theta_b = -0.5$ mrad	8.5 cm	265 °C
Beam angled by $\Delta_y \theta_b = +0.5$ mrad	58 cm	275 °C

TABLE II. Results for the maximum temperature in the absorber for different electron beam configurations in the FLUKA simulations.

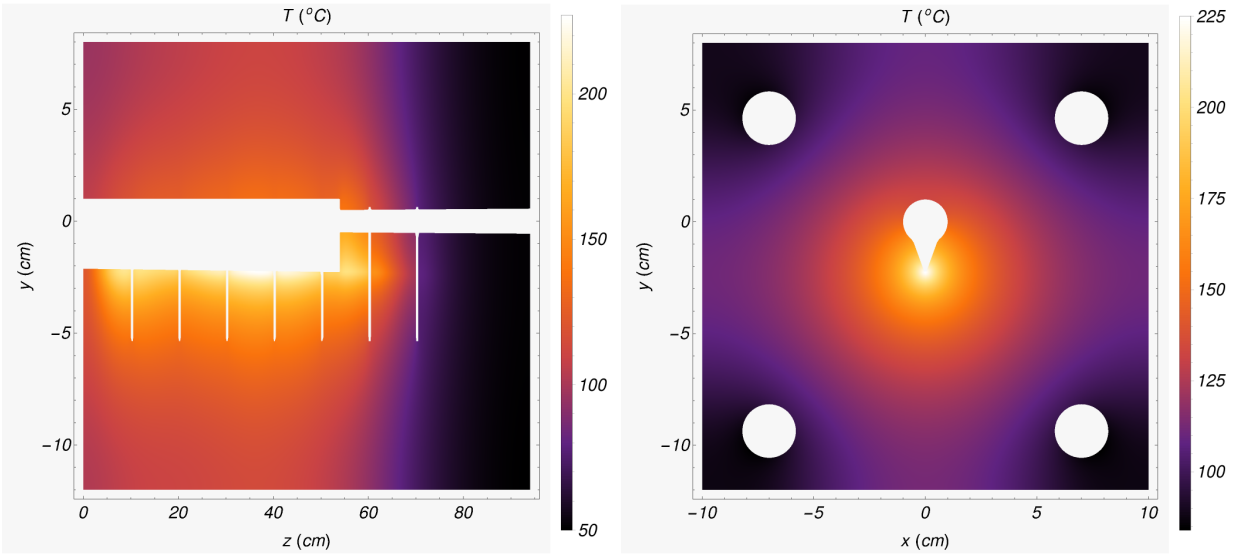

FIG. 19. Expected temperature of the CPS absorber calculated using Wolfram Mathematica [9] for the nominal beam conditions. Left panel: Temperature versus y- and z-coordinates in the vertical mid-plane $x = 0$. Right panel: Temperature versus x- and y-coordinates in the vertical plane at the hot spot location $z = 37$ cm.

design when these parameters are optimized, will most likely be different.

The temperature distributions in the absorber obtained using Wolfram Mathematica [9] assuming four cooling pipes with radius of 1.2 cm are shown on Fig. 19. Note, that the primary electron beam is at the elevation of $y = 0$ cm. The temperature hot spot is at the bottom of the beam cavity at the very beginning of the absorber. For that reason the

center of the absorber in the transverse direction is chosen to be at the bottom of this cavity and not at the elevation level of the primary electron beam. According to Fig. 19, the maximum temperature in the copper absorber is expected to be on the order of 230 C° at the nominal beam conditions, which is very far from the melting point of copper. With the assumed water temperature and the heat exchange coefficient, the highest temperature at the surface of the cooling pipes is expected to be at around 100 °C. The left panel of Fig. 20 shows the temperature distributions versus z-coordinates along the horizontal line $(x, y) = (0.0 \text{ cm}, -2.25 \text{ cm})$. One can see a reasonably flat distribution along the beam direction with the highest temperature point at around $z = 37$ cm. The right panel of Fig. 20 shows the temperature distributions versus y-coordinates along the vertical line $(x, z) = (0.0 \text{ cm}, 37.0 \text{ cm})$ that goes through the hot spot location.

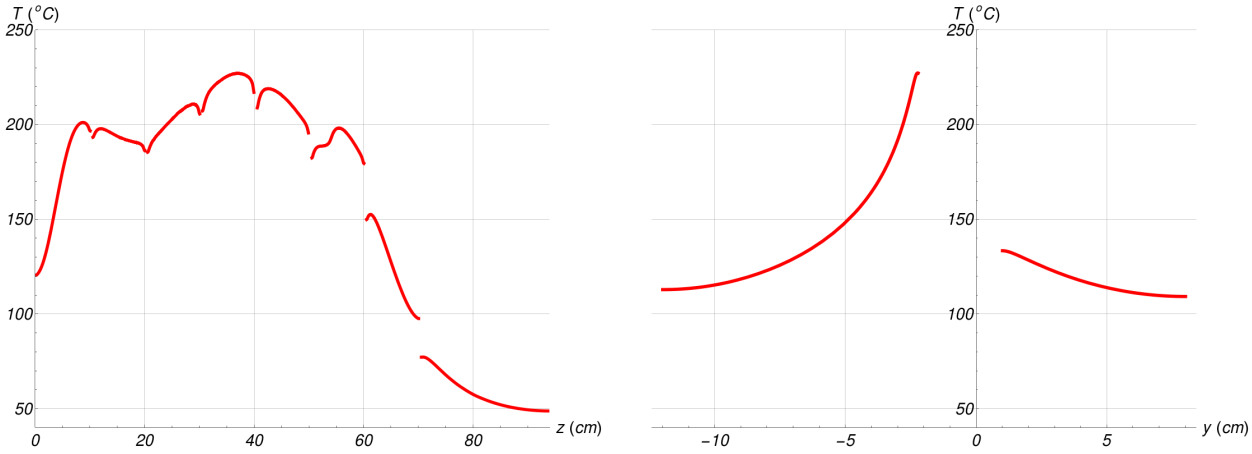

FIG. 20. Expected temperature of the CPS absorber calculated using Wolfram Mathematica [9] for the nominal beam conditions. Left panel: Temperature versus z-coordinates along the horizontal line ($x = 0.0$ cm, $y = -2.25$ cm). Right panel: Temperature versus y-coordinates along the vertical line going through the hot spot location ($x = 0.0$ cm, $z = 37.0$ cm).

In will important for us to monitor the thermal conditions in the copper core of the CPS during the experiment. We plan to install temperature sensors in the absorber that would alert us about deviations from the nominal conditions. Their locations, as well as the locations and the sizes of the cooling channels and the details of the chilled water handling system, will be determined during the engineering design stage. We are considering using the same closed-loop chilled water cooling system that is currently used for the existing Tagger beam dump. At this time the analyses to determine the stresses and the deformations of the absorber using ANSYS [6] are in progress, and the results will be used to optimize the

shape of the absorber such as to minimize the potential risks due to thermal effects.

V. RADIATION LEVELS

A. Prompt Radiation Dose Rate

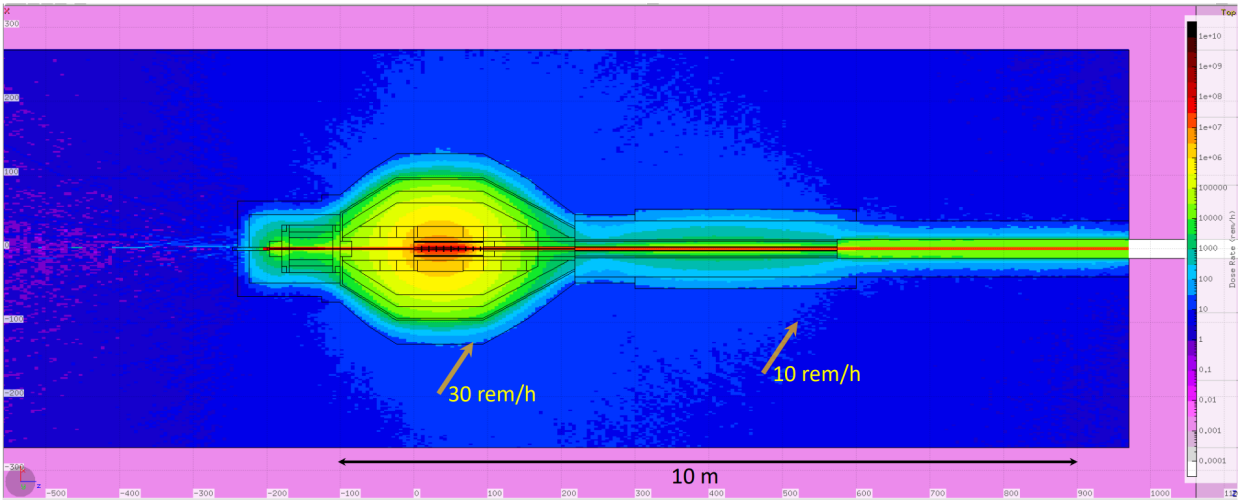

FIG. 21. FLUKA evaluation of the prompt radiation levels in the vicinity of the CPS during nominal experimental running conditions. The color map in Fig. 21 shows the total dose equivalent rate levels in rem/h in logarithmic scale with two variations of color per one order of magnitude in the value. Horizontal cross section of the model is shown. The dose rate map covers the space inside the simulated cylindrical enclosure, surrounded by the concrete walls at radii above 2.7 m, and at z from about -5.7 to 9.7 m in the setup with the coordinate origin at the beginning of absorber. The approximate locations of the prompt radiation levels at 10 rem/h and 30 rem/h are shown by the arrows.

The CPS simulation model described above (see Section III) was used to calculate maps of the prompt radiation fields inside and around the CPS. Fig. 21 illustrates the results of the prompt total dose equivalent rate calculations that are expected to be observed during the operation of the CPS in nominal conditions. The scoring in this plot is done on a grid defined in cylindrical coordinates with the beam axis serving as the z-axis. The scoring volume includes the CPS itself as well as the space around it up to the distance of $r = 2.7$ m. The number of bins in azimuthal angle ϕ is 24 corresponding to a 15° bin size. As the model of the shielding is generally symmetric, averaging of the results over ϕ may characterize the radial dose distributions at various values of z. In this presentation we will use the averaging

of the dose rate map to superimpose it on top of the geometry plane sections within the FLUKA Geometry package, as shown in Fig. 21. At every point in the map the averaging is done in the corresponding (r, ϕ, z) bin, which allows achieving good spatial resolution at small radial distances, and good statistical accuracy at larger radii with larger bin volumes. Using a model with cylindrical shielding layers is advantageous for the development and partial optimization cycle in the conceptual project development, and it will follow with the more realistic implementation of the CPS model in the environment of the Tagger Hall for the final model tune-up and optimization. Fig. 21 plot shows that the level of the equivalent dose rate at 30 rem/h follows approximately the outer surface of main CPS body and the shielding around the permanent magnet. The electrical magnet at the entrance of the CPS is over-shielded in this nominal running configuration, but the shielding is intended for the situations with non-optimal beam, for example, with the beam halo extended beyond $r = 5$ mm. The prompt dose rate levels at $20 - 30$ rem/h correspond to the expected design dose rate levels in the Tagger Hall operations at full beam power, and one of the CPS design goals was to reach that level.

The results may be integrated and averaged over one or two variables in the (r, ϕ, z) set to see the general dependencies in the regions of interest. Figure 22 shows the dependence of the prompt dose equivalent rate around CPS, averaged over the full ϕ-range, and the radial range between 130 cm and 160 cm. The maximum level of about 25 rem/h is observed next to the side of the CPS at the approximate location of the absorber in the center of the CPS.

Fig. 23 shows the dependence of the dose equivalent rate around CPS, averaged over the full ϕ-range, and the range in z from 20 cm to 80 cm, around the maximum. Here we can track the performance of the CPS shielding layers in decreasing the dose rates from very high in the center of absorber, to the acceptable levels at the perimeter. The inner part of the copper absorber experiences full electromagnetic cascades with major sources of the radiation being electrons and photons, then the layers of lead, iron, and barite concrete work to absorb and slow down penetrating high energy neutrons, and the last layer of borated polyethylene finally slows medium energy neutrons down to thermal energies and captures them.

Figures 24, 25, and 26 are similar to Figs. 21, 22, and 23, but with the dose rate scoring volume extending radially beyond the outer concrete and soil wall, and extending forward along the photon beam line until the endpoint where it enters the Collimator Cave. The

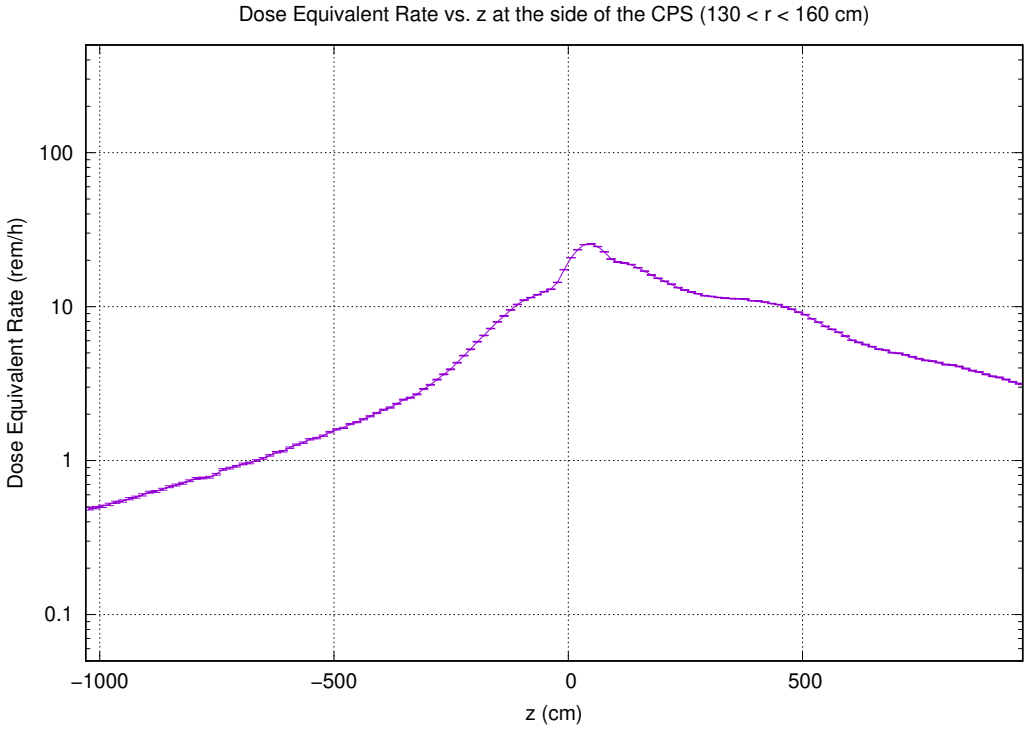

FIG. 22. FLUKA evaluation of the prompt radiation levels in the vicinity of the CPS during nominal experimental running conditions. The total equivalent dose rate levels in rem/h are shown as a function of z, calculated as an average in the radial distance from 130 to 160 cm, along the CPS inside the Tagger Hall.

levels evaluated just outside the outer radius of the soil volume may serve as a conservative estimate of the prompt equivalent dose rate on top of the Tagger Hall during nominal operations. The figure-of-merit of 1 mrem/h corresponds to typically observed levels of radiation during the operations of the high power experimental Halls A and C at Jefferson Lab with acceptable levels of the dose rates observed at Jefferson Lab boundary. The final full simulation of the Hall D KLF setup will include detailed simulations of the dose rates at the boundary. Currently evaluated conservative values of the dose rate on top of Tagger Hall are reassuring us that the contribution of the CPS operation to the boundary dose will be minimal.

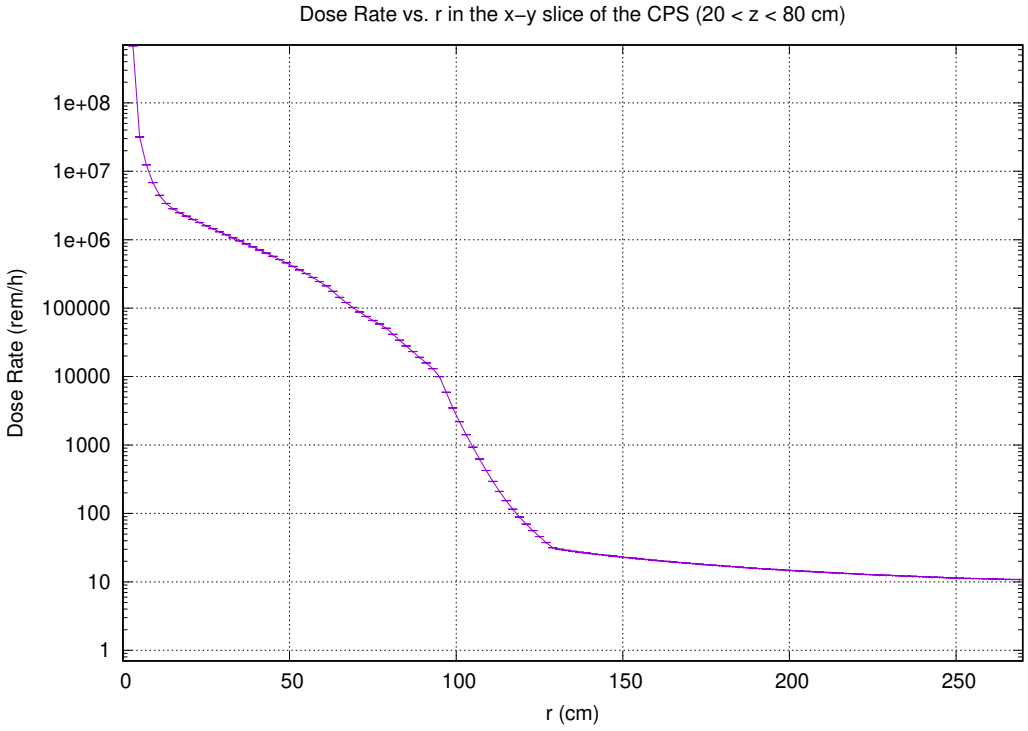

FIG. 23. FLUKA evaluation of the prompt radiation levels inside and in the vicinity of the CPS during nominal experimental running conditions. The total equivalent dose rate levels in rem/h are shown as a function of r, calculated as an average in z from 20 to 80 cm, around the maximum radiation level next to the CPS.

B. Accumulated Dose

Similar to the FLUKA techniques of the prompt dose rate evaluation, as described above in Subsection V A, we create scoring meshes in cylindrical coordinates to calculate the expected accumulated dose and neutron fluence maps around the CPS showing the distributions of the values accumulated over the expected duration of the experiment, conservatively taken as $10,000$ nominal beam hours (about twice of the PAC beam time allocation for KLF). After the FLUKA CPS model run, the distributions are available for superimposing them on to the plane geometrical cuts, and using them to show average values as functions of r and z. These maps will help determine critical areas inside Tagger Hall that should be reviewed in case sensitive electronics and/or materials are planned to be positioned there.

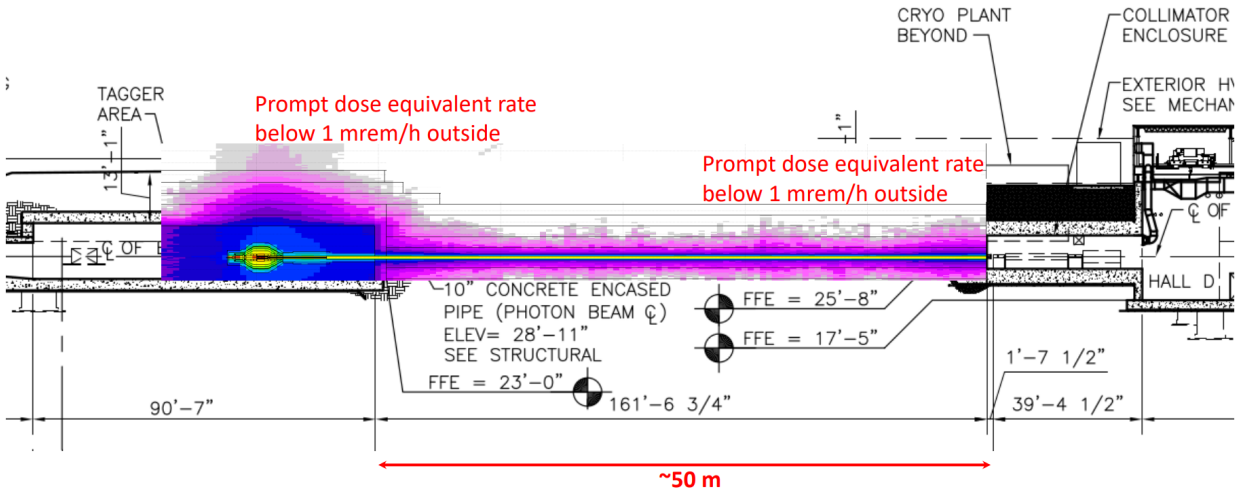

FIG. 24. FLUKA evaluation of the prompt radiation levels extending beyond the Tagger building and outside on top of the shielding berm above the Tagger Hall and above the photon beam line during nominal experimental running conditions. The color map and the CPS geometry are superimposed onto the vertical cut in the engineering drawings showing both Tagger building and the part of Hall D including the Collimator Cave. The color scale corresponds to the total equivalent dose rate levels in mrem/h in logarithmic scale with two variations of color per one order of magnitude in the value. The two color levels visible outside and above the berm correspond to the levels below 0.3 mrem/h and below 1 mrem/h.

Figure 27 shows the accumulated dose in the vicinity of the CPS after $10,000$ hours of operations at nominal experimental running conditions. The color map shows the dose accumulation levels in Gy in logarithmic scale with two variations of color per one order of magnitude in the value. Horizontal cross section of the model is shown. The dose rate map covers only the space inside the simulated cylindrical enclosure, surrounded by the concrete walls at radii above 2.7 m, and at $z > \approx 9.7$ m from the coordinate origin at the beginning of absorber. The levels of dose accumulation in the vicinity of the CPS in the Tagger Hall are around $100 - 300$ Gy. Figure 28 shows the total dose accumulation levels in Gy in the Tagger Hall as a function of z averaged in r from 130 to 160 cm.

Figure 29 shows the accumulated 1-MeV-equivalent neutron fluence in the vicinity of the CPS after $10,000$ hours of operations at nominal experimental running conditions. The color map shows the neutron fluence accumulation levels in cm^{-2} in logarithmic scale with two variations of color per one order of magnitude in the value. Horizontal cross section of the model is shown. The dose rate map covers only the space inside the simulated cylindrical enclosure, surrounded by the concrete walls at radii above 2.7 m, and at $z > 9.7$ m from the

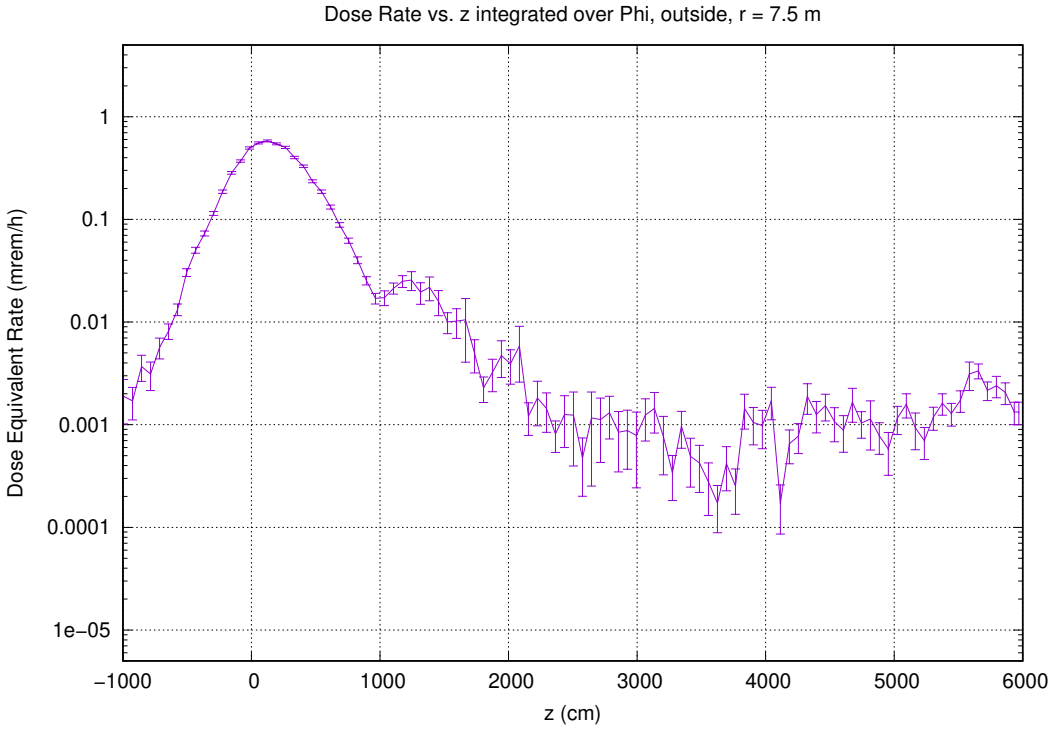

FIG. 25. FLUKA evaluation of the prompt radiation dose rate levels on top of the berm above the Tagger building during nominal experimental running conditions. The total equivalent dose rate levels in mrem/h are shown as a function of z, calculated as an average in r from 750 to 760 cm, along the Tagger Hall and the photon beam line.

coordinate origin at the beginning of absorber. The levels of neutron fluence accumulation in the vicinity of the CPS in the Tagger Hall are around $10^{12} - 10^{13}$ cm^{-2}. The approximate locations of the neutron fluence accumulation levels at 10^{12} cm^{-2} are shown by the arrows. Figure 30 shows the total dose accumulation levels of 1-MeV-equivalent neutron fluence in the Tagger Hall in cm^{-2} as a function of z, calculated as an average in r from 130 to 160 cm.

The resulting levels seem to be reasonable and not unusually high compared to such areas at Jefferson Lab as Accelerator tunnel and high power Halls A and C.

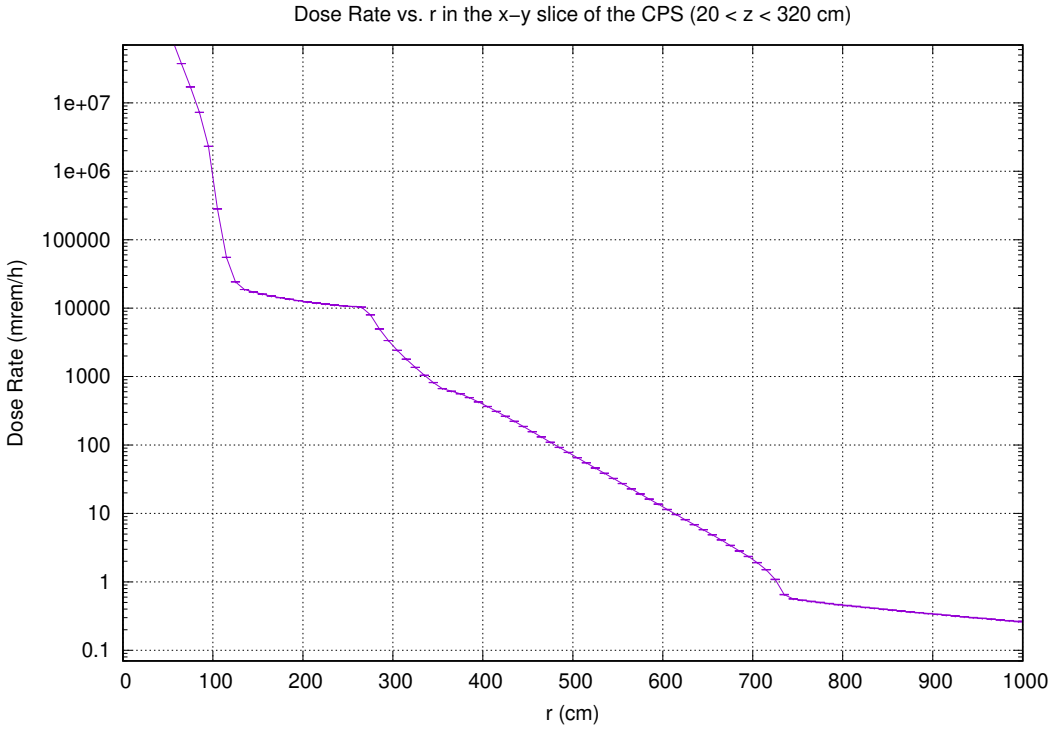

FIG. 26. FLUKA evaluation of the prompt radiation levels inside and in the vicinity of the CPS, radially extending beyond the berm on top of the Tagger building, during nominal experimental running conditions. The total equivalent dose rate levels in mrem/h are shown as a function of r, calculated as average in z from 20 to 320 cm, around the maximum radiation level in the region around the CPS outside. $r = 130$ cm corresponds to the outer radius of the CPS body, at $r = 270$ cm the concrete wall starts, at r above about 730 cm outside air begins.

C. Residual dose rates

Another critical performance parameter of the shielding is the expected residual radiation field around the CPS during beam interruptions and maintenance periods, which may limit access and/or require special mitigation measures before allowing work in its vicinity in Tagger Hall. Conservative goal was established to have such radiation levels to be under the level of 1 mrem/h to 5 mrem/h, 1 hour after stopping beam that was run continuously for $10,000$ hours. Such low levels would allow for personal access to the perimeter of CPS without special designations of "Radiation Areas" or other administrative mitigation measures for workers. Figs. 31 and 32 show the corresponding map and z-dependence of the

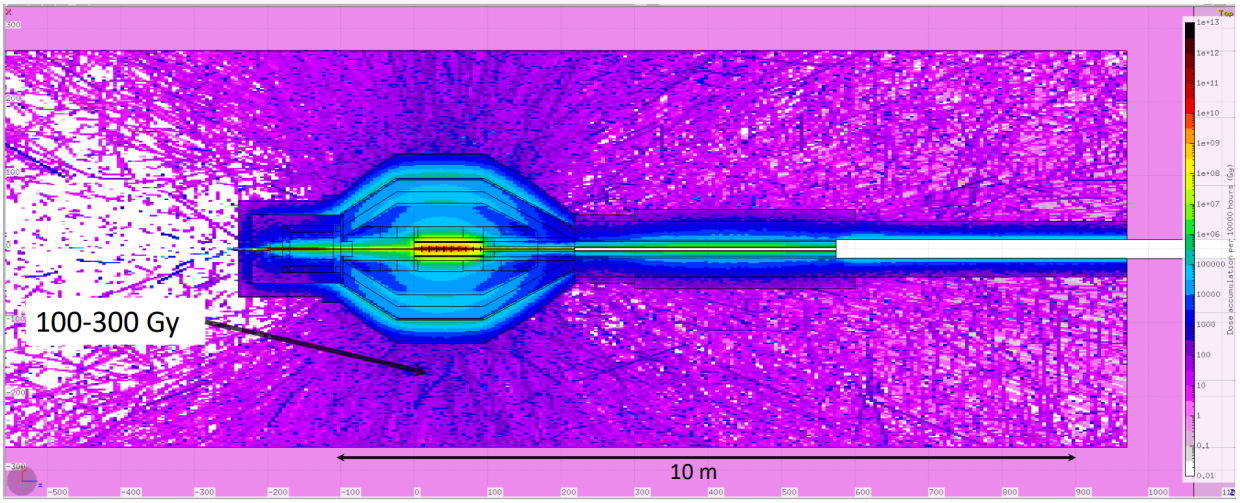

FIG. 27. FLUKA evaluation of the accumulated dose in the vicinity of the CPS after 10,000 hours of operations at nominal experimental running conditions. The color map shows the dose accumulation levels in Gy in logarithmic scale with two variations of color per one order of magnitude in the value. See text for details.

activation dose rate in the vicinity of CPS, one hour after a long continuous run. Apart from the CPS core and the deep layers of lead shielding, the shielding materials contributing to the residual dose rates around CPS are the layers of iron and the high density barite concrete, subject by intense neutron irradiation during the run. The layer of 1 inch lead skin around them, followed by rather thick layer of borated polyethylene keep the dose rates at the CPS perimeter below 1 mrem/h. The choice of the lower limit of 1 mrem/h for the current design is due to systematical uncertainties of 30-50% that may be expected in FLUKA material activation results. The current CPS design satisfies this limit.

D. Lifetime of magnets

Using maps from FLUKA simulations described in Section V B, we can estimate the radiation dose absorbed by the coils of the upstream magnet. Figure 33 shows the map of the accumulated dose in 10,000 hours of continuous operations, zoomed in the regions of the upstream magnet. The boundary between the dark blue and light blue color levels correspond to 10,000 Gy. The four panels show front, top, side, and front views of the cut planes each crossing the magnet coils, similar to the top left panel in Fig. 11. The values of the calculated dose accumulation are placed on top of the coil contours in all the panels.

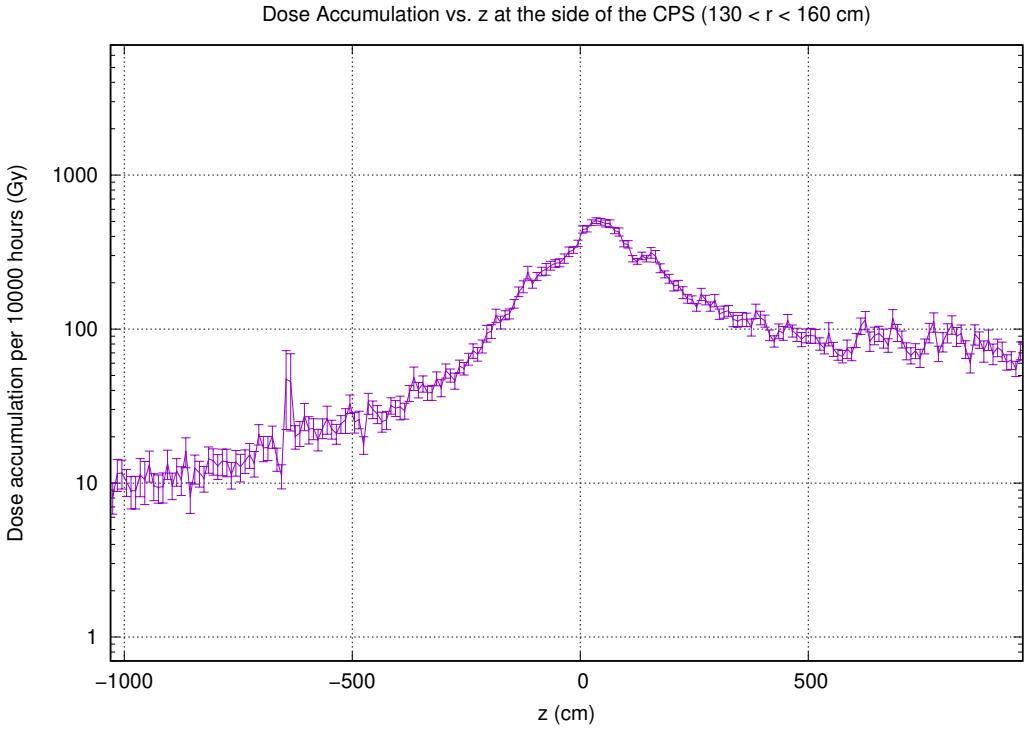

FIG. 28. FLUKA evaluation of the accumulated dose versus z in the vicinity of the CPS after 10,000 hours of operations at nominal experimental running conditions. See text for details.

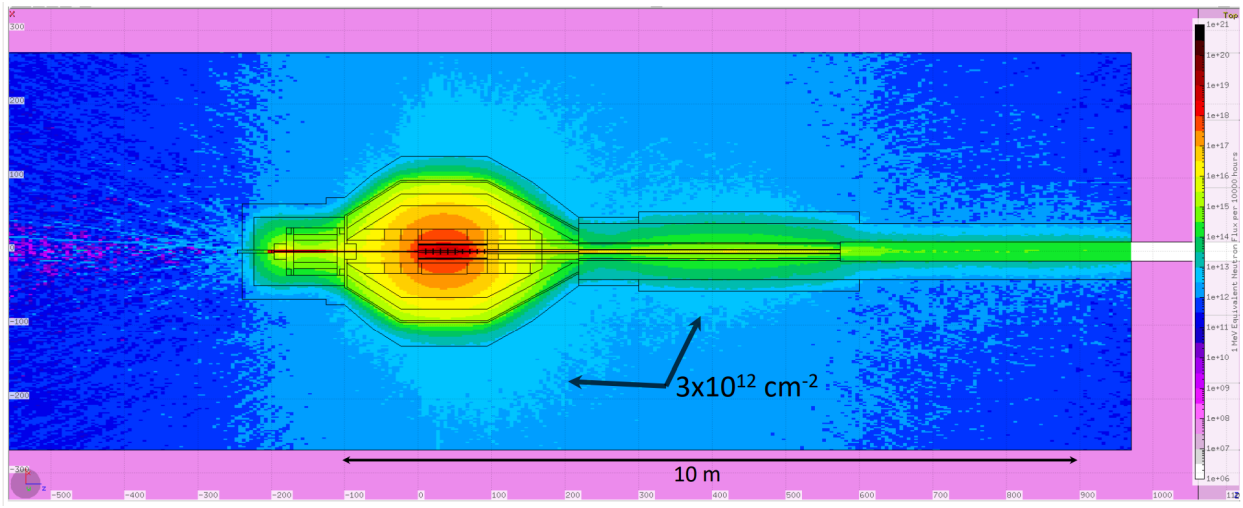

FIG. 29. FLUKA evaluation of the accumulated 1-MeV-equivalent neutron fluence in the vicinity of the CPS after 10,000 hours of operations at nominal experimental running conditions. See text for details.

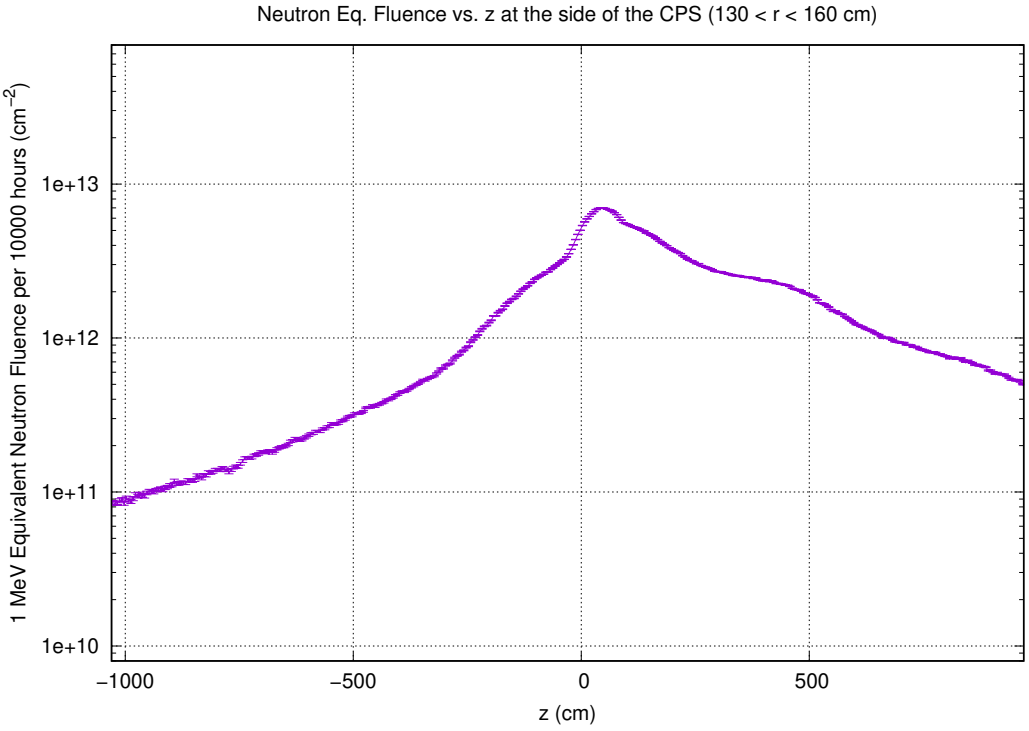

FIG. 30. FLUKA evaluation of the 1-MeV-equivalent neutron fluence in the vicinity of the CPS after 10,000 hours of operations at nominal experimental running conditions.

The levels of the dose accumulation is the lowest at the coils at the CPS entrance (smallest z, top left panel). The values increase to the downstream end of the magnet, up to just under $\approx 30,000$ Gy while it was shown that modern coil insulation made of cyanate ester resins can handle well over 10^7 Gy dose [10].

Similarly, we can estimate the accumulated dose in the permanent magnet downstream of the CPS. Figure 34 shows the accumulated dose in the areas in and around the permanent magnet at the exit of the CPS after 10000 hours of operations at nominal experimental running conditions. The color map shows the dose accumulation levels in Gy in logarithmic scale with two variations of color per one order of magnitude in the value. The boundary between the dark blue and light blue color levels correspond to 10,000 Gy. The four panels show front (at $z = 270$ cm), top (at $y = 0$ cm), side (at $x = 0$ cm), and back (at $z = 440$ cm) views of the cut planes. The values of the calculated dose accumulation are placed on top of

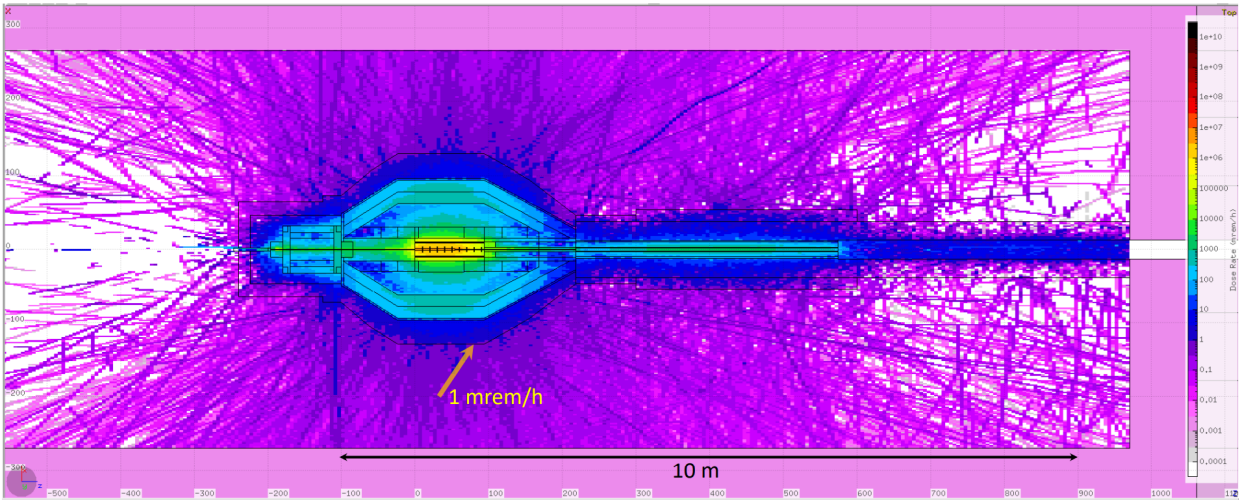

FIG. 31. FLUKA evaluation of the radiation levels in the vicinity of the CPS from the material activation, 1 hour after a long continuous run at nominal experimental running conditions (10,000 hours). The color map shows the total equivalent dose rate levels in mrem/h in logarithmic scale with two variations of color per one order of magnitude in the value. Horizontal cross section of the model is shown. The dose rate map covers only the space inside the simulated cylindrical enclosure, surrounded by the concrete walls at radii above 2.7 m, and at $z > 9.7$ m from the coordinate origin at the beginning of the absorber. The approximate locations of the prompt radiation levels at 1 mrem/h are along the color transition shown by the arrow, roughly corresponding to the outer CPS surface.

the plots. The levels of the dose accumulation is smaller upstream at $z = 270$ cm, and reaches its maximum closer to the end at $z = 440$ cm. The values do not exceed $\approx 3 \times 10^7$ Gy in the areas close to the beam, and stay much lower in the bulk magnet volume. The magnetic field of Hall D strontium ferrite is not expected to change at such doses, and the specifications of the magnet [8] provide only an upper limit of less than 1% change in the magnetic field after receiving a dose of 10^7 Gy.

VI. BEAM CHARACTERISTICS

A. Electron Beam

The proposed KLF experiment will be conducted using 12 GeV electron beam at 5 μA current that will need to be well tuned to pass through the narrow beam channel at the upstream end of CPS and make impact on the copper core in the designated area. Instabilities on the beam parameters, such as beam current and beam positions, may have

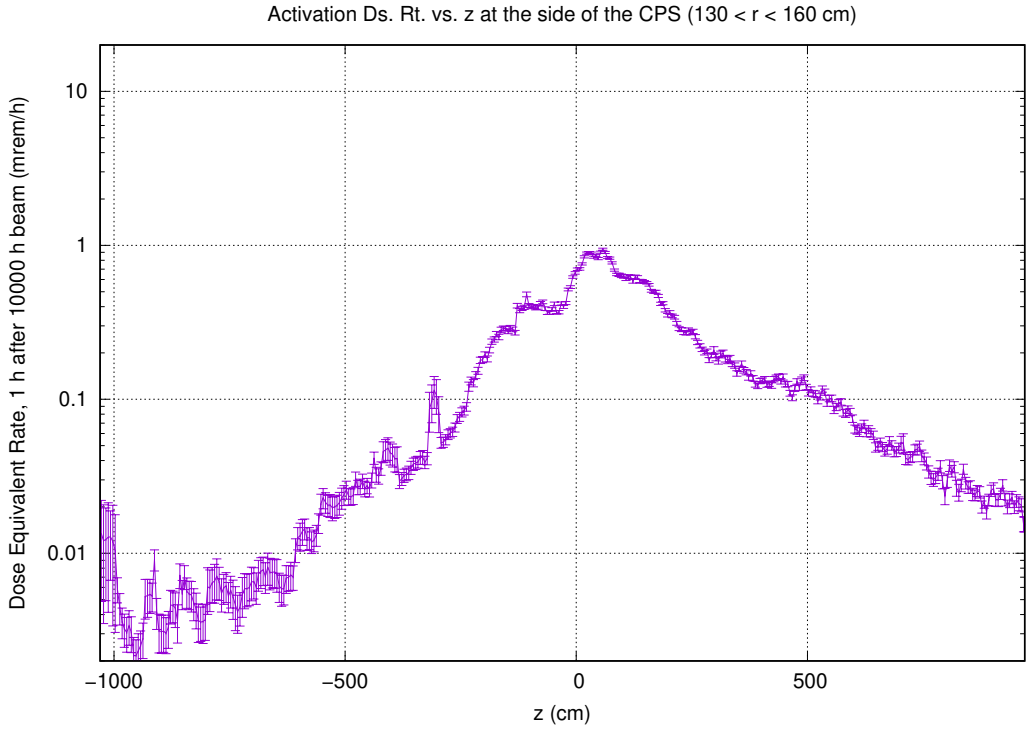

FIG. 32. FLUKA evaluation of the radiation levels in the vicinity of the CPS from the material activation, 1 hour after a long continuous run at nominal experimental running conditions (10,000 hours). The total equivalent dose rate levels in mrem/h are shown as a function of z, calculated as average in r from 130 to 160 cm, along the CPS inside the Tagger Hall.

negative effects on the performance of the CPS. We will need to install a beam current monitor (BCM) upstream of CPS radiator to know the amount of beam current delivered to the hall in order to avoid excessive power being deposited into the CPS. As mentioned in the previous sections, large beam excursions can cause excessive heat in the absorber as well as higher radiation dose rates around CPS. With that in mind, hereby we specify beam requirements for operating CPS during KLF experiment that are summarized in Table III and are described in subsections below.

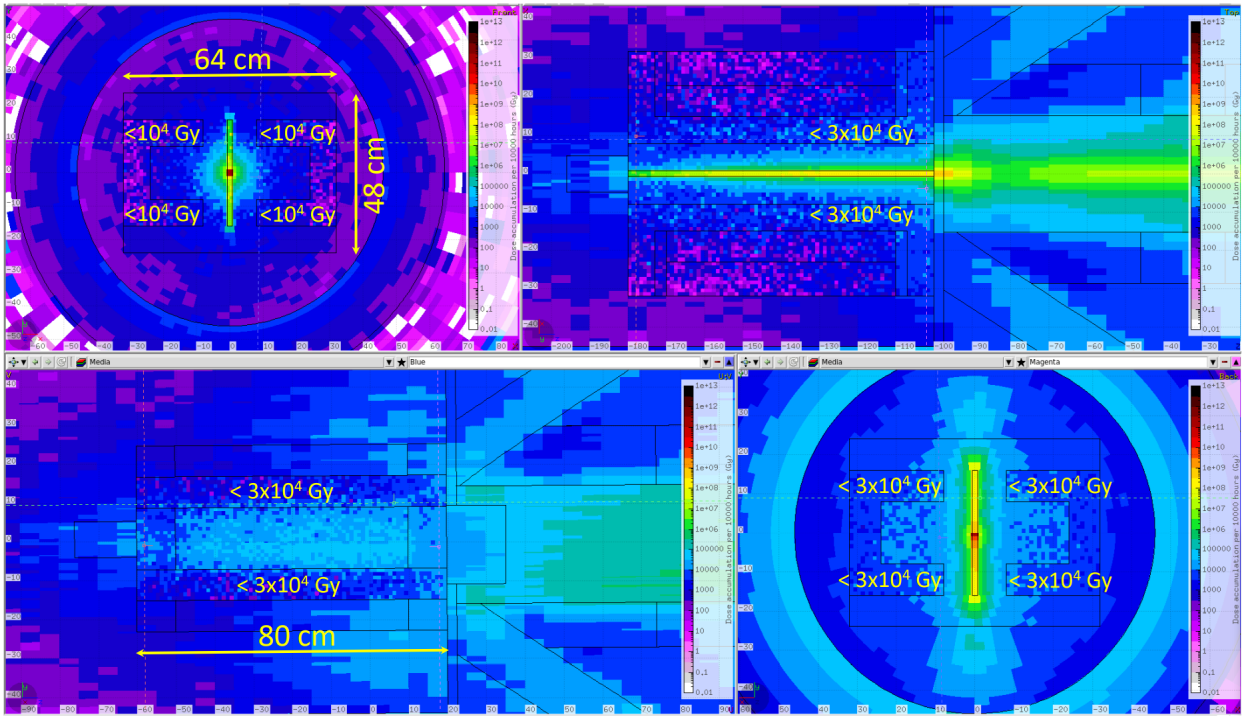

FIG. 33. FLUKA evaluation of the accumulated dose in the areas in and around the powered magnet at the entrance of the CPS after 10,000 hours of operations at nominal experimental running conditions. The color map shows the dose accumulation levels in Gy in logarithmic scale with two variations of color per one order of magnitude in the value. See text for details.

Parameter	@Radiator	@KPT
Beam Current	$50\ \text{nA} \leq I_B \leq 5\ \mu\text{A}$	N/A
Beam Size	$0.5\ \text{mm} \leq \sigma \leq 1.5\ \text{mm}$	$\sigma \leq 1\ \text{cm}$
Beam stability (@ 1 Hz)	$\sigma \leq 0.2\ \text{mm}$	$\sigma \leq 2\ \text{mm}$
FSD is tripped at	$\lvert\Delta x\rvert > 1\ \text{mm}$ or $\lvert\Delta y\rvert > 1\ \text{mm}$	$\lvert\Delta x\rvert > 1\ \text{cm}$ or $\lvert\Delta y\rvert > 1\ \text{cm}$
Beam halo (halo-to-peak)	$< 10^{-4}$	N/A

TABLE III. Specifications for the electron beam for Hall D CPS.

1. *Beam Positions at the Radiator*

Due to the small size of the beam channels in CPS, the beam positions at the radiator will need to be measured using a strip-line beam position monitor (BPM) installed just upstream of CPS. We would like to have the electron beam locked to the nominal positions near the radiator with stability of $\sigma \leq 0.2$ mm, similar to the specifications of GlueX experiment. Based on GlueX experience, we do not expect a fast feed-fack system to be

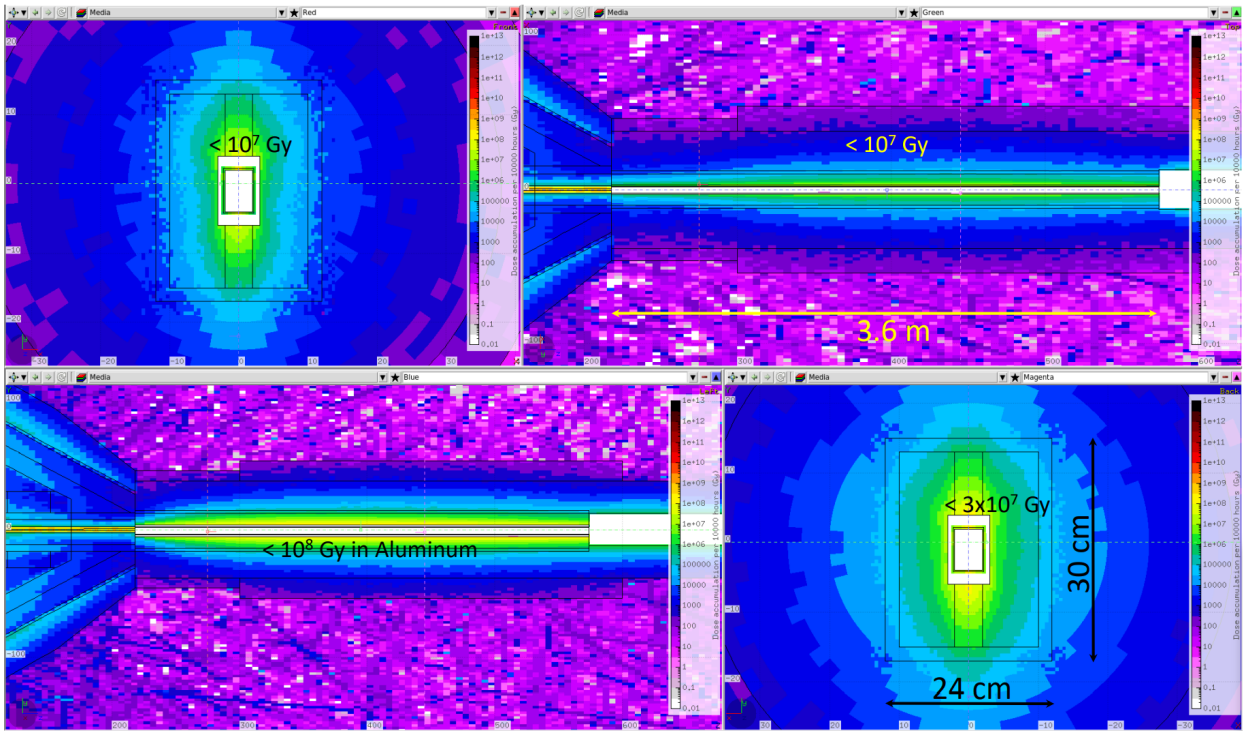

FIG. 34. FLUKA evaluation of the accumulated dose in the areas in and around the permanent magnet at the exit of the CPS after 10000 hours of operations at nominal experimental running conditions. The color map shows the dose accumulation levels in Gy in logarithmic scale with two variations of color per one order of magnitude in the value.

necessary for providing beam position stability at higher frequencies. The desired nominal size of the electron beam for KLF at the radiator is $\sigma = 1$ mm in both horizontal and vertical directions as this is the beam profile (Fig. 35) for which we optimized the CPS design. The acceptable range for the transverse size of the electron beam in front of the radiator with the current CPS design is 0.5 mm $\leq \sigma \leq$ 1.5 mm for both horizontal and vertical widths. The lower limit on the beam size is dictated by the need to reduce the maximum temperature in the absorber, while the high limit of the width is due to possible excessive radiation inside and outside of the CPS.

In the course of our studies we determined that large electron beam excursions on the face of the radiator can produce high temperatures at the upstream end of the copper absorber. To prevent them from happening, we can monitor the beam positions at the entrance of CPS during the experiment and communicate any instability in the beam positions to the operators at the CEBAF Machine Control Center. In addition, we propose to install a narrow beam collar with a length of a few radiation lengths at the entrance of the CPS to

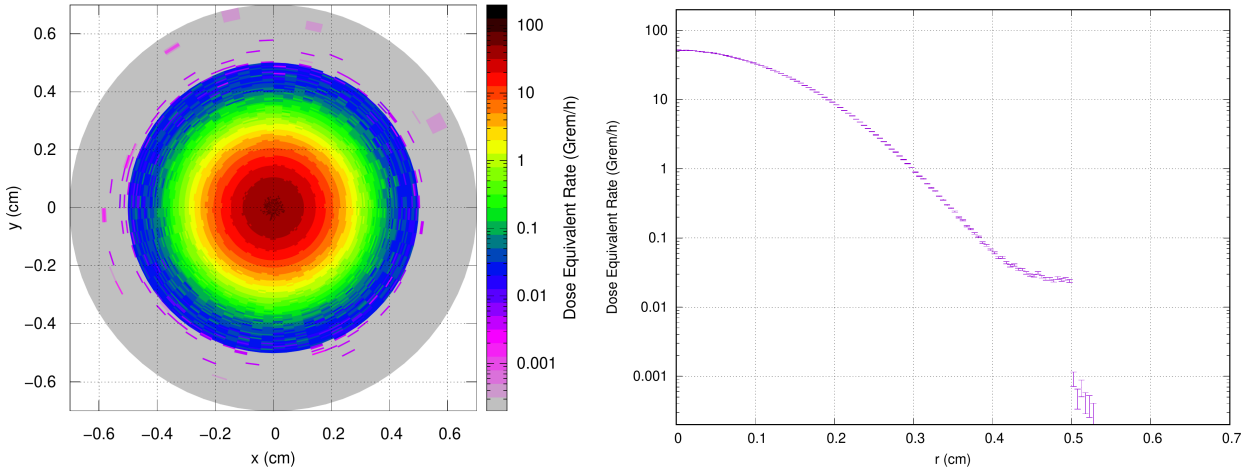

FIG. 35. Nominal electron beam profile on top of a 10^{-4} beam halo radially extending to 5 mm at the entrance of CPS used in the FLUKA simulations. Left panel shows the dose rate equivalent at the entrance to CPS in units Grem/h versus x and y coordinates. The right panel shows the dose rate equivalent versus radial distance from the center of the beamline.

create secondary particles from interactions of the Gaussian tails of the beam with the collar during beam excursions larger than 1 mm. The excessive ionizing radiation will be detected by a standard ion chamber similar to ones that are widely used at CEBAF which will be plugged into one of the Fast Shut-Down (FSD) inputs of the FSD board in the Tagger Hall. The collar will need to be specifically designed for a given transverse size of the electron beam, and the FSD trip levels will need to be established before production running, and may need to be periodically adjusted for the best performance. Such a setup can also help us tune the electron beam to the center of the CPS radiator by varying the beam positions measured in the BPM in front of CPS and minimizing the signal from the radiation monitors positioned near the beam collar.

2. Beam Halo

During standard GlueX beam operations with the diamond radiator, the electron beam profile is normally about 1 mm wide in the horizontal direction and approximately 0.5 mm wide in the vertical direction. It is rare that there are visible shoulders or bumps on the sides of the main peaks of the beam in the measurements performed using the Hall D "radiator harp" scanner that has more than 10^4 of dynamic range. Presence of beam halo during KLF above the level of 10^{-4} with respect to the main peak or extending radially beyond 5 mm

from the beam center may result in elevated radiation levels upstream of CPS, and it may also produce higher radiation exposure for the coils of the CPS magnet. Large halo will also negatively impact the sensitivity of our proposed setup for detecting large beam position excursions as it will produce larger background levels, see Section VI A 1. Therefore, we plan to measure the beam profile with the Hall D wire scanner on a daily basis to detect presence of beam halo and ask CEBAF Machine Control Center for beam adjustments if there is excessive halo observed.

3. Beam Direction

If the electron beam angle at the entrance to the CPS deviates from its nominal value by a large amount, on the order of ~ 0.5 mrad, the main interaction point of the beam with the absorber will drift further along the beam and will create a hot spot with elevated temperatures, see Table II. Such large deviations of the incident angle will result in a very large offset, on the order of ~ 3 cm, of the photon beam spot on the beryllium target in the Collimator Cave. We propose to install a device similar to the Active Collimator used by GlueX experiment to monitor photon beam positions [4] in front of the Kaon Production Target assembly. We would like to use the signals from this device to have a position lock with stability of $\sigma \leq 2$ mm at the face of Kaon Production Target. In addition to the position signals for continuous position monitoring, the KLF version of Active Collimator would also need to produce discriminated signals that can be used in the FSD inputs.

As discussed in Section II B, the position of the beam impact point on the absorber linearly depends on the magnetic field strength. Changes of the magnetic field on the level of a few percent can cause the hot spot to move along the beam direction either to the upstream face of absorber channel, or downstream to the position where the conical photon beam channel begins. In either case, we expect elevated temperature levels which would like to avoid. In order to avoid such incidents, we propose to use the current measurements in the CPS magnet power to trigger a Fast Shut-Down of the beam if the current deviates from the nominal value by more than one percent. We can also install pick-up coils inside the upstream magnet to detect sudden changes in the magnetic field to turn off the beam to the hall.

B. Photon Beam

Our FLUKA simulations also allows us to evaluate the photon beam quality provided by the proposed CPS model. Figure 36 shows the dose equivalent rate distributions at the location of the Kaon Production Target (KPT) versus the transverse coordinates. The left panel shows the dose equivalent rate versus x in a narrow slice of y from -2 mm to 2 mm. The right panel shows the dose equivalent rate versus y in a narrow slice of x from -2 mm to 2 mm. The dose equivalent rate effectively reflects the energy weighted distributions for the photons exiting the photon beam line and entering the Collimator Cave.

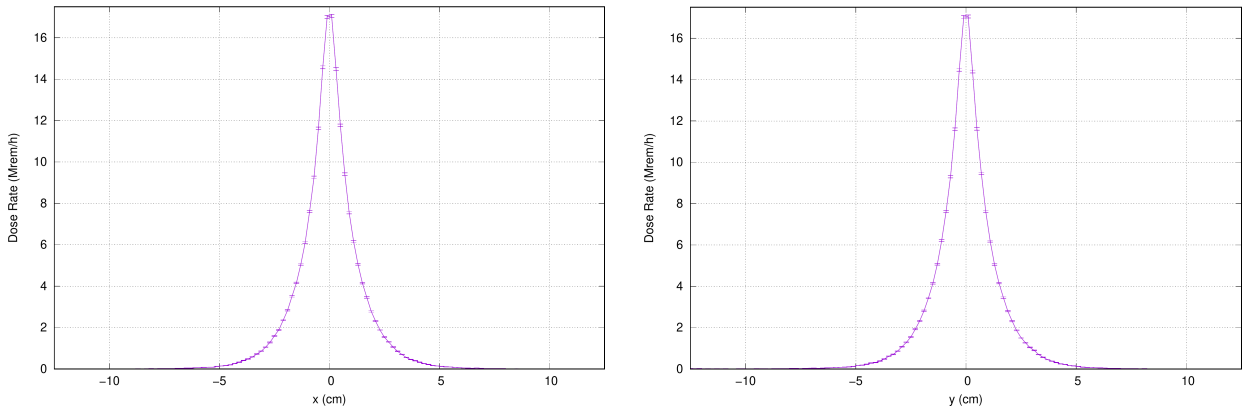

FIG. 36. FLUKA simulation results for the dose equivalent rate distributions as a function of horizontal (left) and vertical (right) coordinate at the entrance of the Collimator Cave in a narrow slice in the orthogonal coordinate from -2 mm to 2 mm.

Figure 37 shows the energy weighted energy spectra of photons, charged particles, and neutrons exiting the photon beam line and entering the Collimator Cave, normalized per one incident beam electron. The value of the normalized energy weighted photon spectrum as a function of photon energy is close to a constant at ≈ 0.1, corresponding to the radiator thickness at 10% R.L., illustrating good quality of the photon transmission line. The contamination of the exiting photon beam with charged particles (green) and neutrons (black) is negligible at relative levels below 10^{-3} and 10^{-6}, mostly observed at lower energies.

VII. SUMMARY

We proposed a conceptual design for Compact Photon Source that would satisfy the requirements of the KLF experiment [1] in Hall D. We used FLUKA code [5], which is one

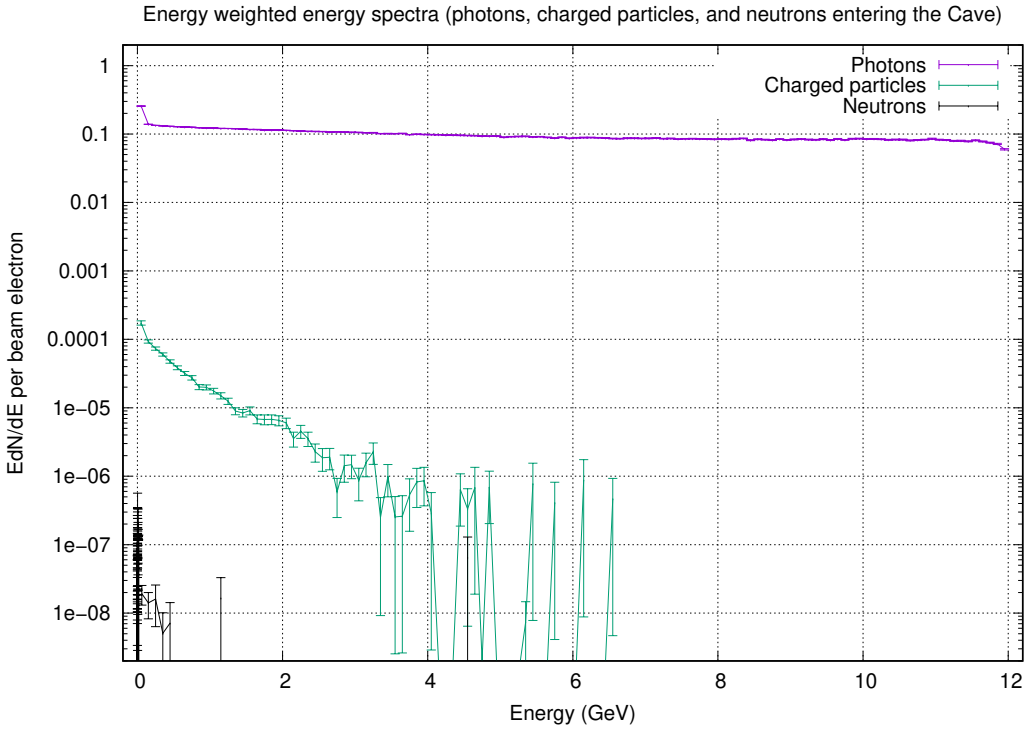

FIG. 37. FLUKA simulation results for the energy weighted energy spectra of photons, charged particles, and neutrons exiting the photon beam line and entering the Collimator Cave, normalized per one incident beam electron. See text for details.

of the most reliable software tools for predicting the radiation environment, to evaluate the dose rates in the Tagger Hall. By evaluating the power deposition of the electron beam in the copper absorber using FLUKA simulations and solving the Poisson equation with ANSYS [6] and Wolfram Mathematica [9], we estimate that the maximum temperature in the absorber will be between 200°C and 300°C when running with a realistic electron beam that is within the KLF specifications. In order to prevent potential contamination due to activated cooling water, we propose to use a close-circuit chilled water system, similar to what is currently used for the Tagger dump, for cooling the CPS absorber.

Based on our simulations, we predict that the prompt dose equivalent rate around CPS is expected to be on the level of $\sim$ 20 rem/h which is similar to the radiation level that is expected to be present in the Tagger Hall if Hall D ran with 5 μA electron beam current on the nominal GlueX diamond radiator [1]. The prompt equivalent dose at the boundary

of the Tagger Hall above the berm is not expected to exceed 1 mrem/h. Therefore, no civil construction around the Tagger Hall will be required to operate the CPS model presented in this document. We also estimated that the residual dose rate around CPS after $10,000$ hours of continuous KLF beam operations and one hour cool-down period will be on the level of 1 mrem/h, which is below requirements of the Radiation Control Group of Jefferson Lab. The radiation doses that the new electrical magnet and the existing permanent magnet will receive during the entire KLF run are expected to be too low to cause noticeable deterioration of their performances.

ACKNOWLEDGMENTS

We would like to thank Tanja Horn, Rolf Ent, Gabriel Niculescu, Steven Lassiter, and Donal Day for fruitful discussions and valuable suggestions. This material is based upon work supported by the U. S. Department of Energy, Office of Science, Office of Nuclear Physics under contract DE–AC0506OR23177.

---

[1] Moskov Amaryan et al. Strange Hadron Spectroscopy with Secondary KL Beam in Hall D, 2021. arXiv:2008.08215.

[2] Igor Strakovsky, Moskov Amaryan, Mikhail Bashkanov, William J. Briscoe, Eugene Chudakov, Pavel Degtyarenko, Sean Dobbs, Alexander Laptev, Ilya Larin, Alexander Somov, and Timothy Whitlatch. Conceptual Design of Beryllium Target for the KLF Project, 2020. arXiv:2002.04442v1.

[3] D. Day, P. Degtiarenko, S. Dobbs, R. Ent, D.J. Hamilton, T. Horn, D. Keller, C. Keppel, G. Niculescu, P. Reid, I. Strakovsky, B. Wojtsekhowski, and J. Zhang. A conceptual design study of a Compact Photon Source (CPS) for Jefferson Lab. *Nuclear Instruments and Methods in Physics Research Section A: Accelerators, Spectrometers, Detectors and Associated Equipment*, 957:163429, Mar 2020.

[4] S. Adhikari et al. The GlueX beamline and detector. *Nuclear Instruments and Methods in Physics Research Section A: Accelerators, Spectrometers, Detectors and Associated Equipment*, 987:164807, Jan 2021.

[5] T. T. Böhlen, F. Cerutti, M. P. W. Chin, A. Fassò, A. Ferrari, P. G. Ortega, A. Mairani, P. R. Sala, G. Smirnov, and V. Vlachoudis. The FLUKA Code: Developments and Challenges for High Energy and Medical Applications. *Nuclear Data Sheets*, 120:211–214, 2014.

[6] ANSYS, Inc. Ansys Mechanical , Finite Element Analysis (FEA) Software for Structural Engineering. https://www.ansys.com/.

[7] Dassault Systèmes. OPERA, Electromagnetic and Electromechanical Simulations. https://www.3ds.com/products-services/simulia/products/opera/.

[8] FNAL. The Fermilab Main Injector Technical Design Handbook, August 1994. FERMILAB-DESIGN-1994-01.

[9] Wolfram Research, Inc. Mathematica, Version 13.1. Champaign, IL, 2023.

[10] P.E. Fabian, J.A. Rice, N.A. Munshi, K. Humer, and H.W. Weber. Novel Radiation-Resistant Insulation Systems for Fusion Magnets. *Fusion Engineering and Design*, 61-62:795–799, 2002.